WAGENINGEN UNIVERSITY AND RESEARCH

METEOROLOGY AND AIR QUALITY

MSC THESIS

Evaluation of Colombian methane emissions combining WRF-Chem and TROPOMI

Author

Joost VERKAIK

Supervisor

Laurens GANZEVELD

July, 2019

Abstract

Methane (CH_4) is, after CO_2, the most important anthropogenic greenhouse gas, contributing to 18% of anthropogenic radiative forcing and mixing ratios are increasing fast. In the early 2000s, the satellite SCIAMACHY observed a large enhancement of XCH_4 over Colombia, but to this day it is uncertain what causes these high values of methane. This thesis aims to get a better understanding of the contribution of different methane sources to this enhancement, by comparing model simulations in WRF-Chem with high-resolution satellite measurements from TROPOMI. The model simulations include the most important emission sources of methane: biomass burning (GFED), anthropogenic (EDGAR) and wetland emissions (LPX). The seasonality of the natural sources is investigated by comparing the dry season (January) with the wet season (August). TROPOMI shows that there is still a similar enhancement of XCH_4 present over Colombia. The comparison between the WRF simulated- and TROPOMI measured XCH_4 shows large differences. Especially the northwestern part of Colombia shows large differences in both the wet and dry season, with an underestimation in WRF's XCH_4 of over 75 ppb. These differences are probably caused by an underestimation of emissions by wetlands, agricultural activity and fossil fuel exploitation. Another interesting result is found in the Orinoco region. In August, when wetland emissions in this area are highest, the model simulations agree reasonably well with TROPOMI, but the comparison for January shows an unexpected result. The January 2019 TROPOMI XCH_4 measurements show relatively large methane enhancements, but it is expected that wetlands do not emit methane during the dry season. The impact of fossil fuel emissions are tested, by using a different inventory regarding these specific emissions. This results in a slightly improved representation of the simulated XCH_4, but only confined to a small area around Lake Maracaibo. Lastly, the missing emissions to match the TROPOMI observed XCH_4 are estimated. This shows that methane emissions have to increase by a factor 10 over northwest Colombia to achieve the observed XCH_4 enhancement. This presented study shows that methane emissions for the investigated domain focused in and around Colombia are substantially underestimated by the used inventories, since the simulated enhancement in XCH_4 was smaller than the observed enhancement. It must be further investigated which of the different methane sources are mostly contributing to this inferred discrepancy between the TROPOMI observed- and WRF simulated enhancement in methane.

Acknowledgements

First I would like to thank Laurens Ganzeveld for supervising me during this thesis. I also want to thank all the members from the MAQ thesis ring for all the helpful feedback. Next, I want to thank everyone who provided me with all the data that is used in this thesis. Alba Lorente helped a lot with the processing of the TROPOMI data and making it available for me. Sander Houweling provided the LPX wetland emission inventory, which was very important for this project. I also want to thank Marcela Quiñones for sending me the very nice inundation and land use maps. Lastly, I want to thank Tia Scarpelli for providing me the fuel exploitation emission inventory.

Contents

1 Introduction

1.1 Background

Methane (CH_4) is the second most important anthropogenic greenhouse gas, after carbon dioxide (CO_2). It is responsible for around 18% of anthropogenic radiative forcing (Forster et al., 2007). Since the industrial revolution, methane mixing ratios have increased by 150% to a global surface average of 1751 ppb in 1999 (Bousquet et al., 2006; Dlugokencky et al., 2003). After this increase, methane mixing ratios remained fairly constant until 2007. The reason for this change in growth rate is still quite uncertain (Nisbet et al., 2014; Turner et al., 2017). After 2007, methane started rising again to the current global average surface mixing ratio of 1866 ppb (Rigby et al., 2008; Dlugokencky, 2019). Besides the direct contribution to radiative forcing, methane also plays an important role in the atmospheric oxidation capacity. Chemical interactions with methane contribute to the production of tropospheric ozone and stratospheric water vapor, who in turn also add to radiative forcing (Forster et al., 2007; Hansen and Sato, 2001). Another reason for the importance of methane for mitigation measures, is the relatively short lifetime of CH_4 compared to CO_2. CO_2 has a lifetime ranging from 50 years to several hundreds of years (Archer et al., 2009), while methane has a much shorter lifetime of approximately 9 years (Nisbet et al., 2016). This difference makes it an interesting greenhouse gas for mitigation measures, since methane has relatively short-term impacts on climate.

Despite the importance of methane for the Earth's climate and atmospheric chemistry, the spatial patterns of the global sources and sinks of methane are not sufficiently understood. One of the most important sources of atmospheric methane are wetlands. Wetlands are soils that are periodically or permanently flooded with water. They contribute approximately 40% to global CH_4 emissions (Walter and Heimann, 2000). Of this 40%, it is estimated that 50% is represented by tropical wetlands (Ringeval et al., 2014). These tropical wetlands are not only important for the global burden of methane, but they also have a large impact on the interannual variability in methane concentrations. This is also due to the dependence of these wetland emissions on soil temperature and soil moisture (Christensen et al., 2003). Several studies suggest a strong positive feedback of CH_4 emissions from wetlands to global warming (Pandey et al., 2017; Nisbet and Chappellaz, 2009; Petrenko et al., 2009). Therefore it is important to get a better understanding about the distribution and magnitude of these emissions. Besides natural emissions of wetlands, important anthropogenic sources of methane are energy production, farmed ruminant animals, rice agriculture and biomass burning. The most important sink of atmospheric methane is oxidation by hydroxyl radicals (OH). This accounts for about 90% of the total methane sink (Kirschke et al., 2013). An overview of the estimated CH_4 sources and sinks is presented in Table 1.

Knowledge about the global distribution of atmospheric methane strongly increased with the launch of methane measuring satellites. The SCanning Imaging Absoption spectroMeter for Atmospheric CHartographY (SCIAMACHY) on board the European Space Agency's environmental research satellite ENVISAT was the first space-based instrument to measure the column average mixing ratio of atmospheric CH_4,

Table 1 | Global methane budget. Estimated sources and sinks of atmospheric methane in Tg yr^{-1} for 2000-2009 (Kirschke et al., 2013).

Sources				Sinks	
Natural		Anthropogenic			
Wetlands	217	Agriculture and waste	200	Soils	28
Geological (incl. oceans)	54	Biomass burning	35	Tropospheric OH	528
Fresh water	40	Fossil fuels	96	Stratospheric loss	51
Termites	11			Troposhperic Cl	25
Other	25				
Total natural	347	Total anthropogenic	331		
Total sources			**678**	**Total sinks**	**632**

called XCH_4 (Bovensmann et al., 1999). SCIAMACHY was launched in March 2002 and functioned until May 2012. This instrument provided full global coverage every six days with a resolution of 60 km x 30 km (Frankenberg et al., 2005). After SCIAMACHY, the Japanese Greenhouse gases Observing SATellite (GOSAT) was the only satellite that measured the atmospheric CH_4 burden. GOSAT was launched in January 2009 and is still functioning today. The instrument provides data with a higher spatial resolution compared to SCIAMACHY of 10.5 km x 10.5 km, but with a smaller spatial coverage. GOSAT has a revisit time of 3 days (Yokota et al., 2009).

Observations of the atmospheric methane burden and distribution has been further enhanced with the launch of TROPOMI (TROPOspheric Monitoring Instrument) on board the Sentinel-5 Precursor satellite. This satellite was launched in October 2017 to measure air quality and climate change indicators with a daily global coverage and a spatial resolution of 7 km x 7 km (Hu et al., 2018). More information about this instrument can be found in Section 2.4.

These satellite measurements are especially of large value to quantify the sources and sinks of atmospheric methane in regions that are poorly covered with surface observations.

This thesis focuses on methane emissions in Colombia. Colombia is an interesting area to perform this study, since SCIAMACHY observed a large enhancement of atmospheric methane over this country and surrounding regions (Figure 1). It is still not fully clear what caused this enhancement. Several hypotheses have been proposed, but there is no clear conclusion yet. For example, Keppler et al. (2006) proposed that Amazonian vegetation emits large amounts of CH_4, but this has later been contested after correcting SCIAMACHY observations for spectroscopic errors (Frankenberg et al., 2008). Alternatively, flux measurements by Smith et al. (2000) have shown large seasonal sources of CH_4 over seasonally flooded areas of the Orinoco River Basin in Colombia. It is more likely that these methane sources cause the observed enhancement in

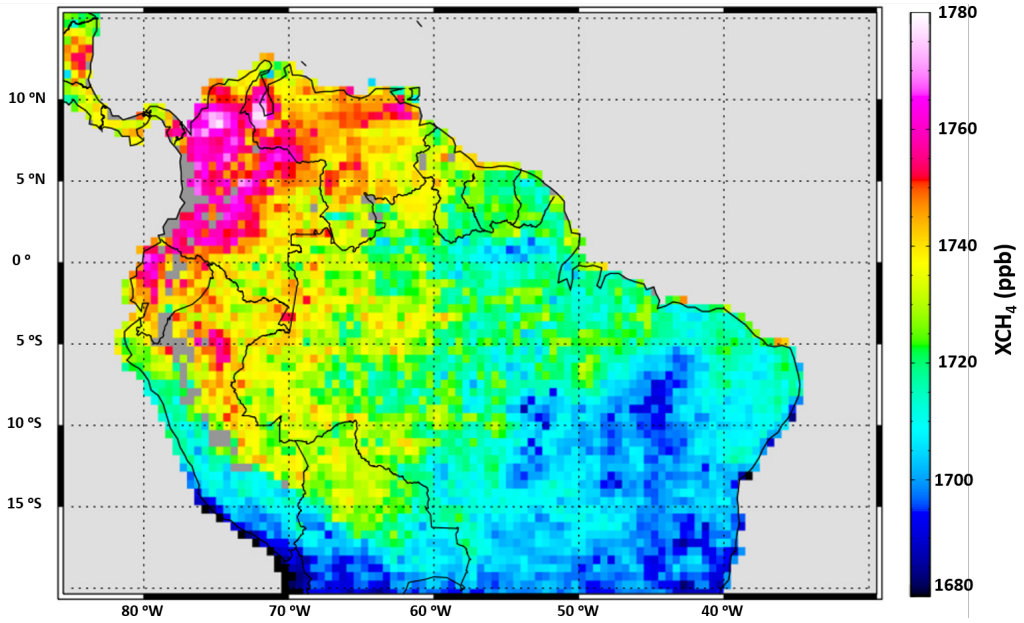

Figure 1 | **SCIAMACHY measurements of XCH_4.** Two-year average (2003-2004) of column averaged mixing ratios (in ppb) of methane observed by SCIAMACHY, where a large enhancement is visible above Colombia (Frankenberg et al., 2006).

the atmospheric CH_4 burden over Colombia, but this is still not studied in sufficient detail to be able to attribute the identified enhancement in XCH_4 over this region to one or more specific sources.

The main anthropogenic sources of methane in Colombia are in the northern half of the country. This part of the country is a mountainous region in which a lot of agriculture takes place. An important part of the agricultural activities in Colombia consists of rice fields, as it covers 30% of the total crop area (Maclean et al., 2013), and thus forming a potential large source of CH_4 (Table 1) over Colombia. In this area there is also meat and dairy cattle, which contribute to the methane emissions as well. Another important anthropogenic source of methane is from the extraction of fossil fuels, like oil, natural gas and coal mining. These sources are located in the north and central part of Colombia, as well as in the northeastern part of Venezuela. These anthropogenic sources are generally assumed to be rather constant in a year, so they do not explain the observed seasonal variation in atmospheric methane. The seasonality is most likely caused by the seasonality in wetland emissions in that area (Chanton and Smith, 1993). Most emissions from wetlands are located in the eastern part and south of Colombia. When the wetlands are flooded, oxygen availability decreases and methanogenic bacteria start producing methane (Neue et al., 1997). Because flooding increases the production of methane, the largest emissions are found in the wet season (Mitsch et al., 2010). This seasonal cycle is also observed in SCIAMACHY satellite observations (Frankenberg et al., 2006). Another source of methane that has a strong seasonal cycle is biomass burning. But this source is less strong and shows an opposite pattern compared to wetlands, as most biomass burning takes place in the dry season (Duncan et al., 2003).

In this thesis, I will conduct meso-scale modelling experiments to consider the contribution of biomass burning, anthropogenic and wetland emissions in determining the established enhancement in methane concentrations over Colombia using WRF-Chem and compare the output with satellite observations by TROPOMI.

1.2 Research objective/questions

The main objective of this study is to evaluate methane emissions over Colombia with satellite measurements of TROPOMI. To reach this objective the following research questions will be answered.

- Do we see an enhancement in atmospheric methane over Colombia in the TROPOMI observations comparable to that observed by SCIAMACHY and if so, how large is the enhancement?
- To what extend is WRF-Chem able to reproduce TROPOMI measurements of methane in Colombia using global inventories for wetlands, anthropogenic sources and biomass burning CH_4 emissions?
- Can we identify possible missing methane sources and estimate its magnitude?
- What is the seasonal variability in the observed methane concentrations and what does this indicate about the role of the natural sources?

2 Data & Methods

This data and methods section is divided into 5 main parts. The first part (Section 2.1), focuses on the WRF-Chem model that is used in this study. The study area and the setup of the model are described as well. In Section 2.2, some of the essentials regarding the used emission databases are described. The inundation data used in the comparison with the wetland emissions is described in Section 2.3. In Section 2.4 we present more details regarding the methane retrieval method of the TROPOMI satellite. Whereas in Section 2.5, we present some specific details on the applied method to address the specific research questions of this thesis study.

2.1 The WRF-Chem model

This study uses version 3.7.1 of the non-hydrostatic and fully compressible Weather Research and Forecasting model coupled with Chemistry (WRF-Chem) (Grell et al., 2005). In this section the study area and the model setup are described.

2.1.1 Study area

Colombia is located in the northwestern corner of South-America and has a very diverse geography. In the western part of the country the Andes mountain range is located (Figure 2), where a lot of agriculture takes place (Armenteras et al., 2011). East of the Andes lies the Orinoco River basin. This is an area that gets flooded during the wet season and is therefore an important source of methane (Smith et al., 2000). The southern half of Colombia consists mainly of tropical rain forest that is part of the Amazon. At the boundary between Colombia and Panama, the Chocó region is located. This area is known for its high amounts of precipitation. The northern tip of Colombia is known as the Guajira region. This is an area where a lot of natural resources, like natural gas, oil and coal, are extracted (Allen et al., 2013).

For my simulations over Colombia, I used a single domain that covers Colombia completely, a large part of Venezuela and parts of Ecuador, Peru and Brazil (Figure 2). The domain has a horizontal grid distance of 27 km and a total area of 2700 km $\times$ 2700 km, centering at 4.89 °N and 71.07 °W. The domain has 30 vertical layers, with the top at 100 hPa. During this study I focused on two different time periods: the wet season and the dry season. In the study area the wet season runs from approximately July until September and the dry season from December until April (Smith et al., 2000). For the wet season simulations I focussed on the analysis of the August observations and model simulations and for the dry season simulations I focused on results for January.

2.1.2 Model setup

In this study, methane is implemented in the WRF-Chem model as a passive tracer. (This is done by using chemistry option 17 in WRF, with CO_2 and CH_4 as greenhouse gas tracers.) Because of the relatively long

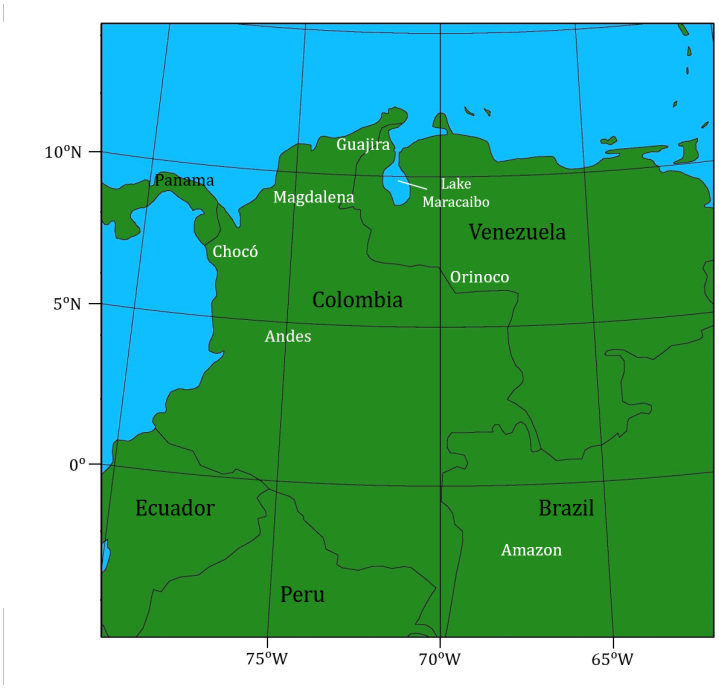

Figure 2 | WRF domain. The domain used in the WRF simulations in this study. Country names are in black and regions that are specifically referred to in this thesis are indicated in white.

lifetime of CH_4 of approximately 9 years (Lelieveld et al., 1998), chemical loss of methane via oxidation is small enough to be ignored in these 1-month simulations. Therefore no chemistry is included. Furthermore, given the relatively small domain size and the role of trade winds in this region, the residence time of CH_4 in this domain is also relatively short. This further justifies to neglect the role of chemical oxidation.

The most important parameterizations that are used are shown in Table 2. For the planetary boundary layer we selected the Yonsei University (YSU) scheme. This parameterization is chosen based on Hu et al. (2010) and Hariprasad et al. (2014), which showed that the YSU scheme describes the boundary layer most accurate in tropic areas. The YSU scheme uses a 1^{st} order closure to calculate the turbulent vertical fluxes within the planetary boundary layer. Betts-Miller-Janjić (BMJ) is selected as cumulus scheme and Morrison 2-moments for the microphysics, based on a study by Reboredo et al. (2015). For the representation of land surface processes, shortwave radiation and longwave radiation the default options are selected, which are respectively Noah LSM, Dudhia and RRTM.

For meteorological boundary conditions data from ECMWF is used based on the year 2014. This provides data every 6 hours with a horizontal resolution of $0.5° \times 0.5°$. The Copernicus Atmosphere Monitoring Service (CAMS) provides the chemical boundary conditions for methane (Massart et al., 2014). The CAMS data is based on satellite observations combined with ground measurements. The chemical boundary conditions are based on 2018.

Table 2 | **Parameterizations.** Parameterization schemes used for the WRF simulations

Parameter	WRF scheme	Reference
Planetary Boundary Layer	YSU	Hong et al. (2006)
Cumulus	BMJ	Betts (1986)
Microphysics	Morrison 2-moments	Morrison et al. (2009)
Land surface	Noah LSM	Chen and Dudhia (2001)
Shortwave radiation	Dudhia	Dudhia (1989)
Longwave radiation	RRTM	Mlawer et al. (1997)

2.2 Emissions

Three different global-scale methane emission databases are used in this study. Emissions from biomass burning are represented by the Global Fire Emissions Database (GFED) (Giglio et al., 2013), the Emissions Database for Global Atmospheric Research (EDGAR) (Crippa et al., 2018) is used for emissions by anthropogenic sources and for wetland emissions the Land surface Processes and eXchanges-Bern Dynamic Global Vegetation Model (LPX hereafter) is used (Ringeval et al., 2014). In this section more information is given about these three different CH_4 emission databases.

2.2.1 GFED biomass burning emissions

The Global Fire Emissions Database (GFED) provides global estimates of emissions from methane and other species and has a spatial resolution of 0.25 x 0.25 degree (Giglio et al., 2013). The inventory provides monthly and daily emission data up to 2016. GFED combines satellite information of fire activity with vegetation productivity to estimate the burned area and fire emissions. Because of the monthly available CH_4 emissions in the GFED inventory the seasonal cycle of biomass burning is present. During the dry season, biomass burning emissions are the highest. The main methane source due to biomass burning is at the Orinoco River basin.

2.2.2 EDGAR anthropogenic emissions

For this study anthropogenic methane emissions from the Emission Database for Global Atmospheric Research version 4.3.2 (EDGAR v4.3.2) (Crippa et al., 2018) are used as input for the WRF model. EDGAR is a joint project from the Joint Research Centre (JRC) from the European Commission and the Netherlands Environmental Assessment Agency (PBL). It provides anthropogenic emissions of greenhouse gases and air pollutants by country and by sector. The data has a spatial resolution of $0.1° \times 0.1°$. EDGAR models the emissions based on the latest scientific knowlegde, available global statistics and methods recommended by IPCC (2006). For the agricultural emission sources, agricultural land use and soil type maps from the

Food and Agriculture Organization (FAO) are used (Janssens-Maenhout et al., 2017). EDGAR v4.3.2 provides annual methane emission data, so no information about seasonal variation of methane emissions by anthropogenic sources is available. Therefore the anthropogenic methane emissions are assumed equal for January and August.

According to EDGAR, the most important anthropogenic sources of methane in Colombia are production by ruminant animals, agriculture and fuel exploitation.

2.2.3 LPX wetland emissions

As mentioned before, wetlands are the most important source of methane in Colombia. In this study, the wetland emissions are based on the LPX-Bern Dynamic Global Vegetation Model that was modified by Ringeval et al. (2014) to represent floodplain hydrology, vegetation and associated CH_4 emissions. This dataset provides monthly global wetland emissions of CH_4 at a horizontal resolution of $0.5° \times 0.5°$.

Originally, the LPX model calculated methane emissions for three different wetland classes: boreal peatlands, inundated wetlands and wet mineral soils. Ringeval et al. (2014) implemented the new class 'tropical floodplain'. The floodplain extend and flooding depth are prescribed using the outputs of the hydrological model PCR-GLOBWB (Van Beek and Bierkens, 2009), which is developed primarily for estimating the availability of fresh water. The main processes that lead to CH_4 emissions are production, oxidation and transport. These are all represented in the original LPX model. The largest modification of the original model by Ringeval et al. (2014) was introduction of the process of a methanogenesis reduction in the presence of oxygen. The modified LPX model calculates this decrease in methane production by calculating the degree of anoxia related to the oxygen concentration and fraction of air in the soil, instead of only the fraction of air in the soil. The total amount of methane being produced by methanogenesis is given by Wania et al. (2010). With this total production of methane by methanogenesis and the reduction of methane due to the presence of oxygen, the methane emissions are calculated.

Ringeval et al. (2014) evaluated the CH_4 emissions computed by the LPX model with flux measurements over the Amazon region. This evaluation shows that the LPX model captures the measured CH_4 fluxes rather well.

2.2.4 CH_4 emission budgets and distribution

Table 3 gives an overview of the emission budgets of the different sources for the domain that is previously shown in Figure 2. Biomass burning has the smallest emission budget of 0.08 Tg/yr for the domain used in the study. The emission budget of anthropogenic sources is already much larger with a total CH_4 emission strength of 10.14 Tg/yr. The largest CH_4 emission source are, as expected, the wetlands with a budget of 26.46 Tg/yr.

The sum of these emissions is used as input for the simulations in WRF-Chem. The total CH_4 emissions for both January and August are shown in Figure 3. The large areas with high CH_4 emissions, for example

the Orinoco area in August, are mainly reflecting the contribution by the wetlands. The small and strong emission sources, like in the northeastern corner of the domain, are emissions by fuel exploitation.

Table 3 | **Methane budgets.** CH_4 budgets of the emission sources in Tg/yr used in the WRF domain

Source	**CH_4 Budget [Tg/yr]**
Biomass burning	0.08
Anthropogenic	10.14
Wetlands	26.46

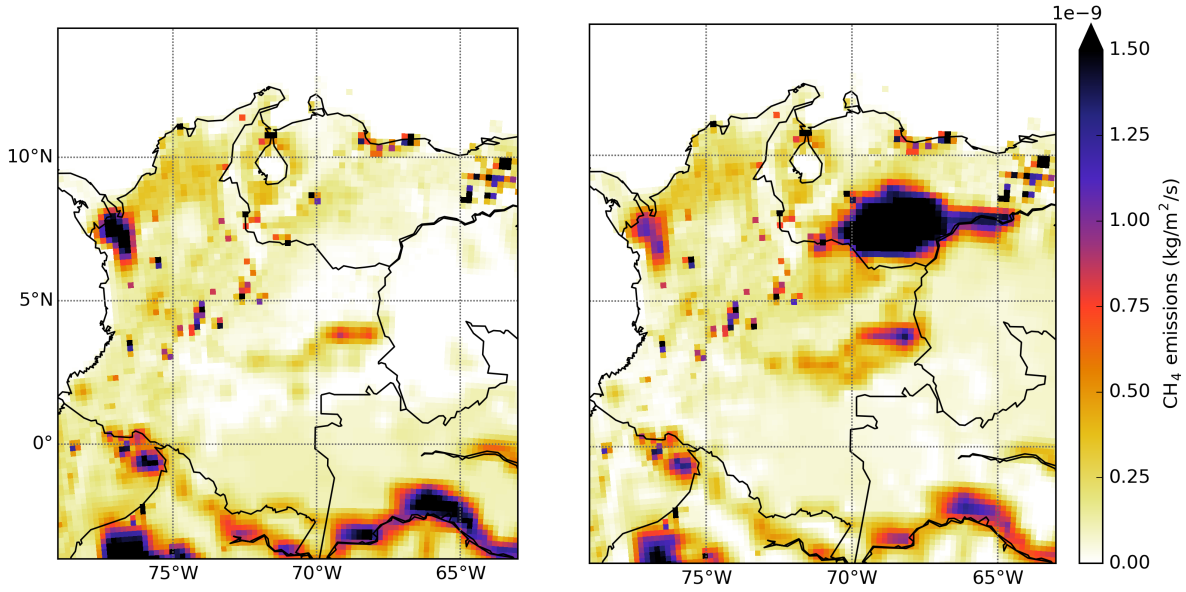

(a) January **(b)** August

Figure 3 | **Emission input for the January and August simulations.** Methane emission input in $kg/m^2/s$ for the WRF-Chem simulations for both January (Left) and August (Right).

2.3 Inundation data

Quiñones et al. (2016) created high-resolution (∼100m) maps of flood frequency and vegetation cover for Colombia. For this maps they used radar remote sensing data from ALOS PALSAR that gives detailed, all-weather, day and night observations at a resolution of 100 meters (Rosenqvist et al., 2007). Given that these radar observations are able to penetrate through the forest canopy, these data contain information both regarding inundation of open vegetation sites as well as flooding conditions below forest canopies. The study period of this project was from 2007 until 2011. For this thesis, the flooding (inundation) data is used for January and August, representing the dry and wet season. The high resolution data have been converted to $0.05° \times 0.05°$resolution for practical reasons, while still keeping the resolution fairly high to still

be able to demonstrate the spatial patterns and heterogeneity in these inundation data.

Since wetland emissions of CH_4 show a strong correlation with the inundation state of the soil, we made a visual comparison between the strength of the wetland emissions according to the LPX inventory and the observed inundation state according to Quiñones et al. (2016).

2.4 TROPOMI retrieval method

On 13 October 2017, the Sentinel-5 Precursor satellite was launched with on board the TROPOspheric Measuring Instrument (TROPOMI). This instrument measures air quality and climate change indicators each day at a high spatial resolution of 7×7 km. Because of the wide swath of 2600 km, it provides full global coverage each day. The local overpass time of the satellite is 13:30h (Hu et al., 2016).

The retrieval algorithm for CH_4 is based on spectroscopic measurements of sunlight in the shortwave-infrared (SWIR) spectral range that is backscattered by the Earth's surface towards the instrument. The absorption lines of CH_4 are used to calculate its atmospheric concentration (Butz et al., 2012). A disadvantage of this method is that it relies on accurate knowledge of the lightpath through the Earth's atmosphere. Scattering by particles, like aerosols, water and clouds, modifies the lightpath and can cause retrieval errors (Frankenberg et al., 2005; Butz et al., 2010). The way these particles modify the lightpath depends on particle amount, type, size and height distribution. This information is not always available. This means that the retrieval method for CH_4 must simultaneously measure trace gas concentrations and the correction for scattering effects.

The end product of the retrieval algorithm is the column-averaged dry air mixing ratio of CH_4, called XCH_4. The algorithm is designed to be efficient and accurate when the atmosphere is cloud-free. So it is important to filter out the data that is measured under cloudy conditions. During this study, this cloud filtering can especially cause data availability problems during the wet season with high cloud cover. Besides the cloud filter, pixels are filtered out when the surface albedo is smaller than 0.02 or for which $f = AOT \times \frac{h}{\alpha} < 110$, where AOT is the Aerosol Optical Thickness, h is the height of the aerosol layer and α is an aerosol size parameter (Hasekamp et al., 2019). Measurements over oceans and other open water bodies are also removed. In principle, it is possible for TROPOMI to get accurate retrievals over oceans, but this will be evaluated in a later phase (Hu et al., 2018).

2.5 Methods

2.5.1 Data preparation

The TROPOMI data is filtered for cloud contamination and other factors. The points that remain have been converted to a $0.25° \times 0.25°$grid and averaged for each month. To compare this re-gridded and averaged XCH_4 columns measured by TROPOMI with the WRF simulations, the WRF output is co-sampled so only the locations that also appear in the TROPOMI data remain. The local overpass time of TROPOMI is around

13:30h, therefore only the WRF output for this time is used in the analysis. To take spin up of the model into account, the first 3 days of the simulations are removed. Because TROPOMI measures CH_4 as column averaged mixing ratios (XCH_4 in ppb), the WRF output is also converted to column averages and averaged over the simulation period of one month. The column average mixing ratio is determined by using the mass of each layer to calculate the WRF column average of the CH_4 mixing ratios. Note that in this calculation we have not applied the averaging kernels from TROPOMI, since these values are typically ranging between 0.98 in the lower kilometers and 1.02 at 10 km altitude. The WRF model only simulates methane mixing ratios up to 100 hPa, while the TROPOMI measurements calculate XCH_4 up to a height of 0.1 hPa (Hu et al., 2016). Therefore the XCH_4 calculated from WRF has to be corrected for the upper part of the atmosphere, which accounts for approximately 10% of the total mass. This is done by estimating the contribution of this upper layer based on vertical profiles of CH_4 from Kenea et al. (2019) and Sugawara et al. (1997). This results in an estimated decrease in WRF's XCH_4 of $\sim$25 ppb. This estimate is comparable to an inferred offset of $\sim$25 ppb base on a comparison of the August TROPOMI and the uncorrected WRF output, shown in Figure 4. Therefore, for the remainder of this study, 25 ppb is subtracted from the WRF simulated XCH_4 for the entire domain.

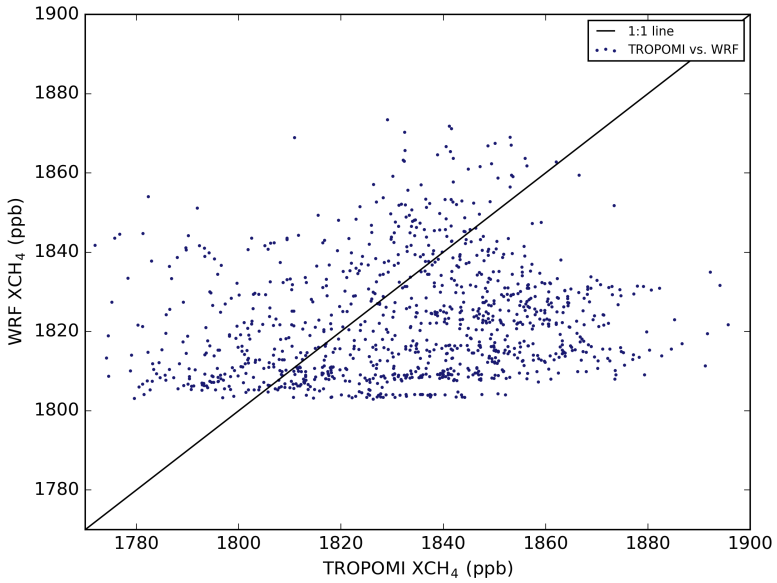

Figure 4 | Scatterplot of uncorrected XCH_4 from WRF and TROPOMI. XCH_4 calculated from the WRF output of August up to 100 hPa on the y-axis. XCH_4 measured by TROPOMI in August 2018 of the x-axis. The black line represents the 1:1 line.

2.5.2 Comparing TROPOMI and WRF

Now both datasets have the same data locations, unit and measuring time, they can be compared using difference plots. This process is done for both the dry and wet season data. By analyzing the difference between the TROPOMI data and WRF simulations, regions that are under- or overestimating methane emissions can be identified. These regions are analyzed further to investigate what possible sources of emissions cause these differences.

3 Results

The first part of this result section (Section 3.1) focuses on the methane measurements by TROPOMI and compares them with previous measurements by SCIAMACHY. After this, the distribution of the most important wetland emissions are compared with inundation data of Colombia (Section 3.2). Next, we take a closer look at the results from the WRF simulations (Section 3.3) and lastly the WRF simulations are compared with TROPOMI measurements (Section 3.4).

3.1 TROPOMI measurements

The first feature from the new TROPOMI methane measurements to be evaluated, is if these new high-resolution XCH_4 measurements show an enhancement like it was observed in the SCIAMACHY data by Frankenberg et al. (2006). To see if there is a similar result in TROPOMI, the monthly mean XCH_4 of August 2018 over Colombia is compared with data measured over a 2-year (2003-2004) period by SCIAMACHY over the same region (Figure 5).

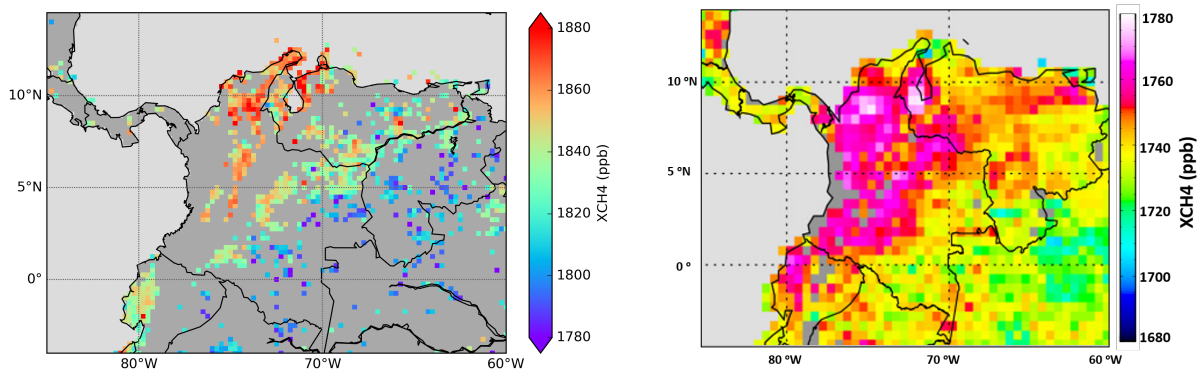

(a) TROPOMI **(b)** SCIAMACHY

Figure 5 | Comparison of TROPOMI and SCIAMACHY. Mixing ratios of CH_4 measured by TROPOMI (a) and SCIAMACHY (b). The TROPOMI data are column-averaged mixing ratios (ppb) of August 2018 gridded with a spatial resolution of 0.25°× 0.25°. The SCIAMACHY data is a 2-year average of column averaged mixing ratios from 2003 and 2004 on a spatial grid of 0.5°× 0.5°(Frankenberg et al., 2006). Grey areas indicate that there is no available data. Note that the color scales and the corresponding values are not the same in both figures.

As you can see in Figure 5a, there are a lot of missing points in the TROPOMI data. This is caused by the strict filtering that is applied to the data (see Section 2.4). Especially the filtering for clouds results in removing many observations.

Just like the SCIAMACHY data, TROPOMI also shows an enhancement over Colombia compared with the surrounding areas. When we compare the absolute values of XCH_4 at the enhancement in both figures, we see that TROPOMI measures values that are around 100 ppb higher than SCIAMACHY did (1880 ppb for TROPOMI and 1780 ppb for SCIAMACHY). This indicates that the column-averaged mixing ratio of

methane has increased by approximately 100 ppb over the last 15 years, which is in agreement with global averaged surface measurements of CH_4 by Dlugokencky (2019).

The magnitude of the enhancement (i.e. the difference between the lowest and the highest value in the domain, ΔXCH_4) measured by TROPOMI has a maximum of $\sim$100 ppb. This agrees reasonably well with an observed maximum enhancement in XCH_4 of $\sim$80 ppb by SCIAMACHY. Even with the limited coverage of the TROPOMI data, we can still see a similar pattern in the methane mixing ratios. The lowest values are found in the southeastern part of Colombia and the highest values are observed in the northwestern part of the country. Besides the general distribution of XCH_4, the highest peaks of XCH_4 are located at approximately the same place in both figures as well. Around Lake Maracaibo in Venezuela and the Magdalena Basin in northern Colombia the highest values are observed by both instruments.

An interesting difference between the two can be observed at northern peninsula of Colombia, the Guajira region. The 2-year averaged SCIAMACHY measurements show relatively low values of XCH_4 in this area, while in the August 2018 TROPOMI data we see values that are high compared to the background values.

3.2 Comparison wetland emissions and inundation data

In Figure 6 the inundation data is compared with the CH_4 emissions by wetlands for both the dry season (January, Figure 6a) and the wet season (August, Figure 6b). The inundated areas are shown in dark blue and the emissions are depicted with three contours. During the wet season, the LPX CH_4 wetland emission database and the inundation data show a reasonable agreement regarding the main locations of more extensive inundated conditions. Especially at the locations in Colombia where the wetland emissions are high (i.e. the red areas in Figure 6b), the density of the inundation data is high. Unfortunately we do not have inundation data from the countries surrounding Colombia, so the strongest sources of wetland emissions in Venezuela and Peru can not be compared with inundation data in terms of seasonal contrasts. However, the smaller emission sources in Colombia (i.e. the green areas in Figure 6b), correspond well with the inundation data. These areas still show some inundation, but the density of these inundation conditions is lower than at the regions with high wetland emissions.

Despite the reasonable agreement of the wetland emissions and the inundation data for the wet season, there are some areas to have a closer look at. For example, we see some areas that show the occurrence of extensive inundation conditions, but are not represented in the wetland emission inventory. The most important example of this is in the northern part of Colombia, around the Magdalena River Basin. Here we see a high density in the inundation data, that is comparable to the inundation state at the high emission regions in Chocó and Orinoco, but the wetland emissions according to LPX are relatively low.

In January, deemed to be representative for the large-area dry season, there is a clear peak in the wetland emission inventory visible over the Chocó region (Figure 6a). The inundation data confirms these high emissions with a high inundation density. After the Chocó region, the most prominent source of methane

in Colombia is located in the eastern part of the country, close to the border with southwestern Venezuela. It is striking to see that the inundation data shows almost no inundation within this emission source area in January, whereas the LPX data still contains some significant CH_4 emissions. Just like during the wet season, the area around the Magdalena River Basin shows also a high inundation density in January. Remarkable to see is that despite it being the dry season, the inundation is even higher than during the wet season. Even with this high inundation state, the CH_4 emissions are fairly low according to the LPX inventory. In January, it is the wet season in the Amazon, opposite to the other areas in the domain. This difference in seasonality is clearly visible in the wetland emission data. In January the emissions over the Amazon are clearly higher than during August. Unfortunately we can not compare most part of this region with inundation data, because this data is only available for Colombia. A small part of the emissions in the Amazon region is over Colombia, and where it is striking to see that over southern tip of the country there is no significant occurrence of inundation conditions for this region for both months.

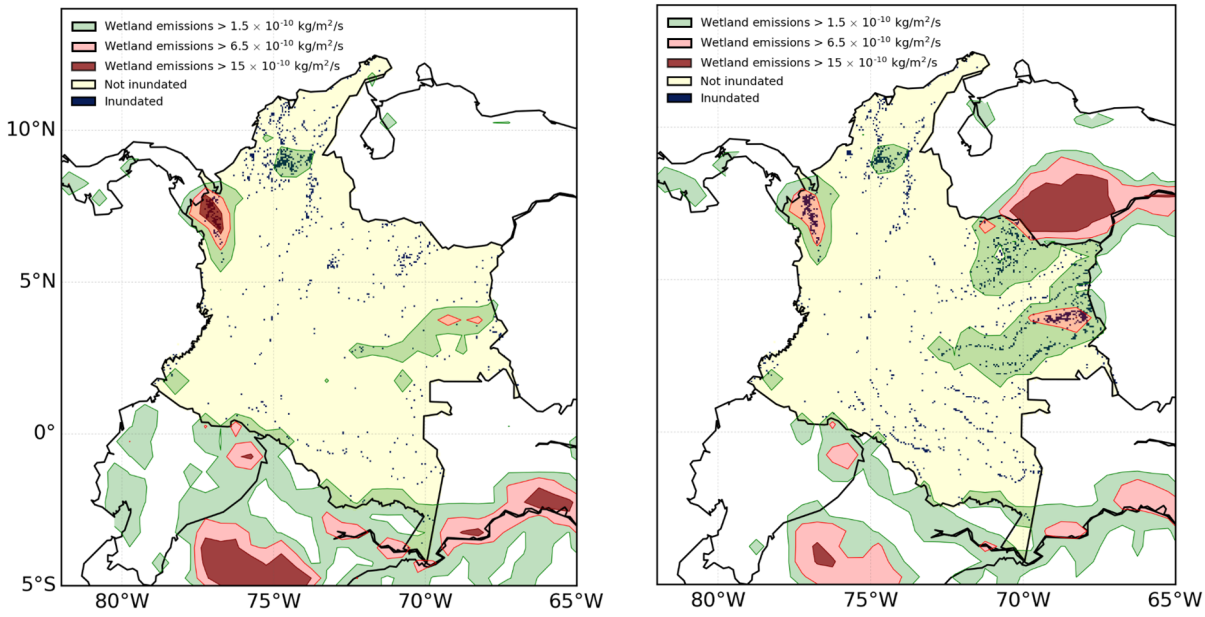

(a) January **(b)** August

Figure 6 | Comparison between wetland emissions and inundation data for the dry and wet season. Inundation data from Quiñones et al. (2016) on a grid of 0.05 degrees with contours of wetland emissions higher than 1.5×10^{-10} kg/m^2/s in green, emissions higher than 6.5×10^{-10} kg/m^2/s in red and emissions higher than 15×10^{-10} kg/m^2/s in dark red for January (a) and August (b). The inundation data for January is measured in 2007, 2008 and 2011 and the data for August is measured in 2007, 2008 and 2010. The inundated areas that are shown were inundated during at least one of these years.

3.3 WRF simulations

3.3.1 August

In the WRF simulations, the high wetland emission clearly cause an enhancement in the column-averaged mixing ratios of CH_4 (Figure 7a). In addition to the simulated XCH_4, Figure 7 also shows the locations where the CH_4 wetland emissions are higher than 6.5×10^{-10} kg/m^2/s with white contours, as well as the monthly averaged 10 meter wind speed and direction. A complete overview of the emissions that are used in the simulation can be found in Figure 3b.

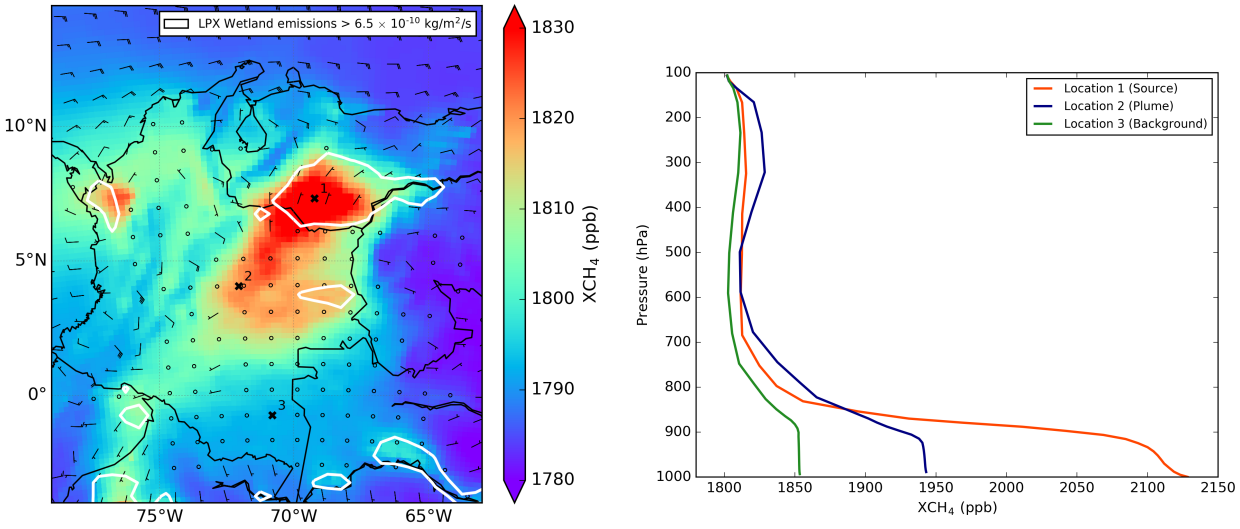

(a) **(b)**

Figure 7 | Simulated XCH_4 of August. *Left:* Simulated XCH_4 (ppb) using WRF for August, with white contours for wetland emissions higher than 6.5×10^{-10} kg/m^2/s and wind barbs for the average 10 meter wind in August, where a half line represents 2.5 knots, a full line 5 knots and a flag 25 knots. *Right:* Vertical profiles of simulated CH_4 at the 3 locations indicated by the crosses in the right figure.

The largest emission source is located in the Orinoco river basin in Venezuela, this area also shows the highest mixing ratios of methane. The dominant wind direction in this region is from the northeast. Eventhough the windspeeds are not very high, it looks like this flow of air causes a simulated enhancement in methane southwest of the emission source. This is confirmed by the simulated vertical profiles of the CH_4 mixing ratios in Figure 7b. The mixing ratio close to the surface is a lot higher directly above the source (red line), but more downwind the CH_4 mixing ratio is higher at higher altitudes in the atmosphere, also pointing at a mechanism of further upward transport of the emitted CH_4 (blue line). This upward transport mechanism is likely convective transport also based on the presence of a second (small) maximum in CH_4 mixing ratios around 200-300 hPa, resembling the typical C-shape distribution in tracers affected by convective transport (Mullendore et al., 2005). The same effect of dispersion of the emitted CH_4 is also visible above the Chocó region, but at a smaller scale. Around this source a dominant westerly wind is

present, which causes the presence of enhanced CH_4 mixing ratios east of the source. The other strong emission sources in the southern part of the domain hardly cause an enhancement in XCH_4. This is probably caused by the boundary conditions prescribed to the model, since these sources are located close to the edge of the domain.

3.3.2 January

The largest difference between the WRF simulations of August and January is the absence of the large enhancement in XCH_4 above the Orinoco region, shown in Figure 8. Just like Figure 7a, Figure 8 also shows the wetland emissions higher than 6.5×10^{-10} kg/m^2/s and the monthly averaged wind speed and direction at 10 meter.

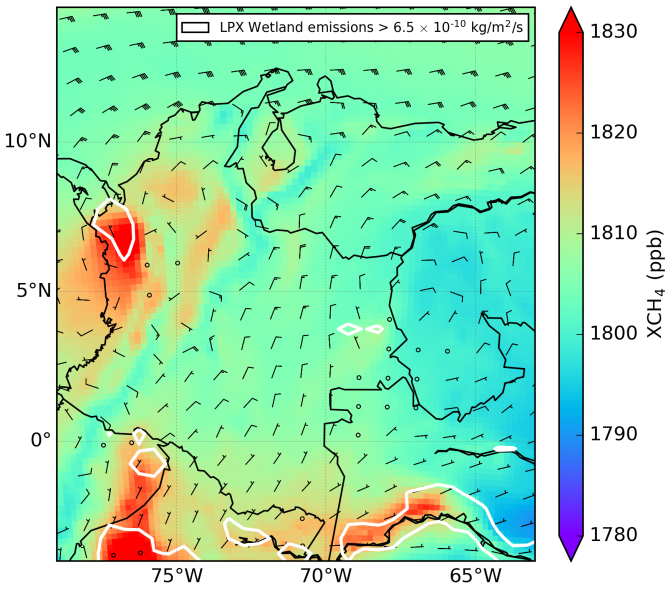

Figure 8 | Simulated XCH_4 of January. Simulated XCH_4 (ppb) using WRF for August, with white contours for wetland emissions higher than 6.5×10^{-10} kg/m^2/s and wind barbs for the average 10 meter wind in January, where a half line represents 2.5 knots, a full line 5 knots and a flag 25 knots.

In January, the strongest source of methane emissions in Colombia are found at the Chocó region, which is known to be one of the wettest places on earth (Poveda and Mesa, 2000). These high emissions cause a large enhancement in XCH_4 directly above the emission source and southwest of the source. Other high values are found over the Amazon and Peru, which have a seasonality opposite to the Orinoco region. So January reflects generally wet season conditions south of Colombia. The small enhancement visible over the Magdalena river valley and Andes region is caused by a combination of smaller wetland emissions and anthropogenic emissions.

The background values in January are around 10 to 20 ppb higher than during the simulation is August. This is also caused by the CAMS boundary condition data that results in imposed enhanced CH_4 mixing

ratios compared to August in the northeastern part of the domain. The wind barbs show a large flow of air from the northeastern corner of the domain towards the west and over the Orinoco region towards the southern boundary of the domain. This flow of air with enhanced methane mixing ratios causes the overall XCH_4 to be around 10 to 20 ppb higher than during August when this inflow of air masses enhanced in methane is less strong.

3.4 TROPOMI compared with WRF simulations

3.4.1 August

One of the first striking features of the comparison between the monthly mean measurements by TROPOMI and the WRF simulations, is that the TROPOMI measurements show much larger values of XCH_4 (Figure 9a and 9b). The mixing ratios from the WRF simulations have a maximum of around 1840, while TROPOMI measures column averaged mixing ratios up to 1880 ppb.

The eastern part of the domain and southern part of Colombia have hardly any emission sources, so observed mixing ratios in these areas can be seen as background values. These background mixing ratios are reasonably similar in both TROPOMI and WRF, with values ranging between approximately 1780 and 1800 ppb.

The area around the Orinoco River Basin also shows values that are reasonably similar in both the TROPOMI measurements and the WRF simulations in this month of August, as both have mixing ratios of approximately 1840 ppb. This is the area with the highest emissions according to the LPX wetland emission inventory, as can be seen in Figure 7. The areas surrounding this large source of methane also show mixing ratios comparable to what is observed by TROPOMI. So it looks like the August wet season wetland emissions in the Orinoco region are reasonably well captured in the LPX emission inventory.

The largest difference that is observed between WRF and TROPOMI, is located in the northwestern part of the domain. TROPOMI measured the highest values of the entire domain in this area, while the emission inventories only contain relatively small emissions. This explains an inferred difference between the WRF-simulated and TROPOMI observed XCH_4 exceeding 75 ppb, which is a difference of approximately 6% relative to the absolute CH_4 mixing ratios. As you can see in Figure 3b, there are hardly any methane emissions in the model in this area in August.

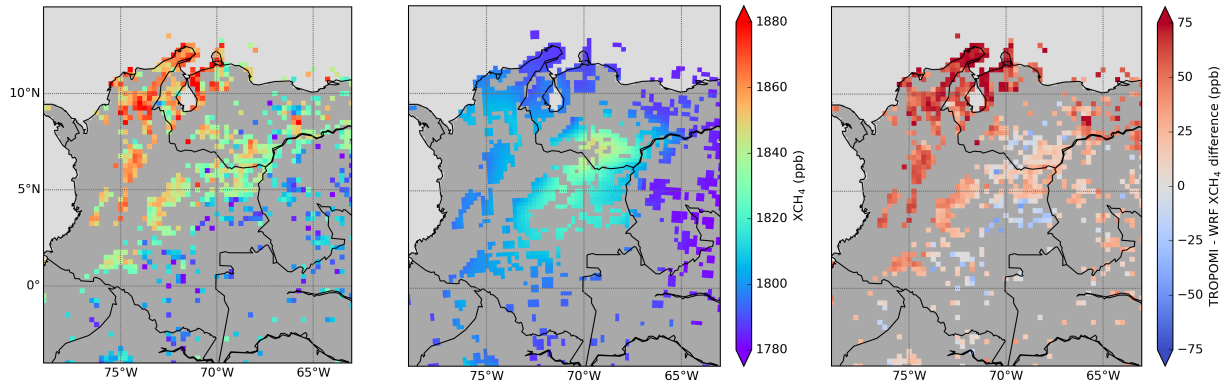

(a) TROPOMI **(b)** WRF **(c)** Difference

Figure 9 | Difference between TROPOMI and WRF for August. Column-average mixing ratios of CH_4 in August 2018, measured by TROPOMI (a) and simulated in WRF (b). Figure (c) shows the difference between TROPOMI and WRF, where red values indicate higher values for TROPOMI and blue values indicate higher values for WRF. The WRF data is filtered to only show the locations that are available in TROPOMI.

3.4.2 January

The comparison between TROPOMI and WRF for January, shown in Figure 10, shows a striking result. The TROPOMI measured XCH_4 are generally substantially higher at almost all locations. Due to a very low TROPOMI coverage, we can unfortunately only compare a few regions, mainly the Orinoco River Basin and the Magdalena River Basin. At both locations large differences are visible. Since it is the dry season in January, we did not expect to see high wetland emissions, but nevertheless the XCH_4 mixing ratios observed by TROPOMI are very high. For the Orinoco region, the values are even higher than during the wet season (Figure 9a).

The WRF simulated XCH_4 shows hardly any horizontal patterns as seen in the limited area over observations by TROPOMI. Since the locations that are included in the TROPOMI measurements are over regions with low wetland emissions according to LPX, there are no real enhancements visible. The Magdalena region shows values that are somewhat higher due to anthropogenic and small wetland emissions in that area, but still very low compared to the TROPOMI data.

Despite the large differences over the Orinoco and Magdalena River Basin, there are some small regions that compare reasonably well. The values in the southern half of Venezuela are reasonably similar in both the TROPOMI measurements and the WRF simulation. These values can be seen as the background mixing ratio of XCH_4. This would indicate that over the other, more westerly located areas in the domain, where the mixing ratios are significantly higher, large sources of methane seem to be present but not being captured by the applied emission inventories.

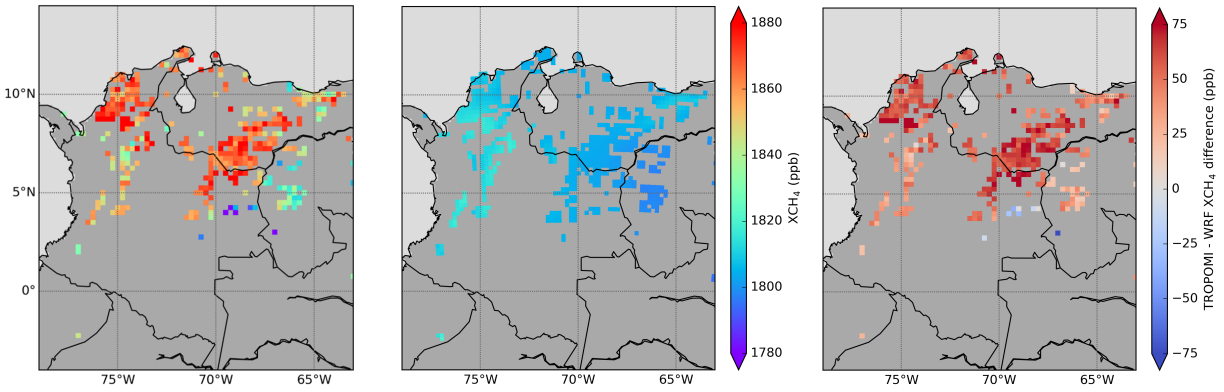

(a) TROPOMI **(b)** WRF **(c)** Difference

Figure 10 | **Difference between TROPOMI and WRF for January.** Column-average mixing ratios of CH_4 in January 2019, measured by TROPOMI (a) and simulated in WRF (b). Figure (c) shows the difference between TROPOMI and WRF, where red values indicate higher values for TROPOMI and blue values indicate higher values for WRF. The WRF data is filtered to only show the locations that are available in TROPOMI.

4 Discussion

This discussion section consists of two main parts. First, possible explanations for the observed differences between the TROPOMI- measured and the WRF simulated XCH_4 are discussed (Section 4.1). For the explanation of the differences we focus on two regions, the northwestern part of Colombia (Section 4.1.1) and the Orinoco River Basin (Section 4.1.2). Next, the results of other simulations are shown to test some hypotheses on missing or misrepresented sources of methane within the study domain.

In the second part of this discussion section, the limitations of the data and methods that are used are discussed. Based on my experiences during this thesis, some recommendations for future research are given. First, limitations and recommendations are given regarding the inundation data and emission inputs for the model simulations. Then, the simulations itself and measurements by TROPOMI are discussed in further detail.

4.1 Differences TROPOMI vs. WRF

4.1.1 Northwest Colombia

The simulated XCH_4 for both the January and August was generally largely underestimated compared to TROPOMI measurements. As we already discussed in Section 3.2, there are areas in the northwestern part of Colombia, around the Magdalena river valley, that show high inundation conditions, but this is not reflected in high wetland CH_4 emissions in the LPX inventory. The inundation conditions also showed that there is no clear seasonal variability in inundation conditions present in the Magdalena river valley with an inferred relatively similar area of inundated conditions for both January and August. This observed absence of seasonal variation is also present in the TROPOMI measurements of XCH_4, which shows substantially enhanced XCH_4 for both January and August. This enhanced XCH_4 is not reproduced by the WRF simulations, which points out a missing source of CH_4 in this region throughout the year. By looking at the peatland distribution in Colombia according to Yu et al. (2010), shown in Figure A.1 in the Appendix, that a large area of the northern Magdalena river basin is covered with peatlands. These peatlands are known to emit methane, although the typical methane fluxes from tropical peatlands have been reported to be less than from tropical wetlands (Couwenberg et al., 2010). In this area there is also palm oil production, as shown in Figure A.2 in the Appendix, and which also provides another source of methane (Yacob et al., 2006). The methane emissions from palm oil production are of a similar order of magnitude as methane emissions from wetlands according to the LPX inventory (Reijnders and Huijbregts, 2008). It must be further investigated to what extent these two sources might pose another significant source of methane in this region and to what extent these sources are indeed, or not, captured in the emission inventory we use in our study. It requires to carefully check if, for example, the agricultural CH_4 emissions of the EDGAR emission inventory also include this contribution by palm oil production.

A different source that might explain the differences observed in this area are anthropogenic emissions

by fossil fuel extraction. The northern peninsula of Colombia, Guajira, and the area around Lake Maracaibo are known for the exploitation of mineral resources, like coal, oil and natural gas, which are known sources of methane (Allen et al., 2013; Warmuzinski, 2008). Emissions from fossil fuel extraction are included in the EDGAR emission database, but it is likely that these are underestimated (Miller et al., 2013; Maasakkers et al., 2019). This hypothesis is further elaborated upon in Section 4.1.3.

4.1.2 Orinoco region

The Orinoco region showed a reasonable agreement between the TROPOMI measured- and WRF simulated XCH_4 for August. However, this region showed large differences in XCH_4 for January, which is representing the dry season (also confirmed by the inundation data), where we do not expect to see significant methane emissions from wetlands. TROPOMI measured an unexpectedly large enhancement of XCH_4 at the Orinoco region in January 2019, with even larger values than those measured in August 2018, while the WRF simulated XCH_4 for January showed no enhancement over the Orinoco region. There are multiple possible explanations for the large enhancement over the Orinoco region during the dry season in 2019. One possibility is the role of methane emissions from biomass burning. During January 2019 there was an El Niño event, which caused dryer conditions than usual (FAO, 2018). This might have caused in increase in forest fires and therefore more emissions of methane. However, because of the low relative contribution of biomass burning to the total emission budget (Table 3), it does not seem feasible that the observed large enhancement in XCH_4 in January 2019 over Orinoco is caused by an enhancement in biomass burning compared to more typical January conditions for this region.

Just like previously stated for the northwestern part of Colombia, a different explanation for the observed large enhancement of XCH_4 over the Orinoco could be the role of methane emissions by oil, gas and coal mining. The northeastern corner of the domain is also a known source of methane by fuel exploitation, and where these emissions might be underestimated by EDGAR v4.3.2 (Scarpelli et al., 2018). Methane emissions in that region will be transported towards the Orinoco region via the northeasterly winds shown in Figure 8. This hypothesis of underestimation of EDGAR's fuel exploitation emissions is tested in Section 4.1.3.

Since the areas with the large enhancement of XCH_4 over the Orinoco region are dominated by wetlands, it is also possible that these wetlands are actually the main cause of the observed the enhancement. Eventhough it is the dry season and the wetlands are not inundated according to the data by Quiñones et al. (2016), maybe they still emit sufficient amounts of methane to result in a significant enhancement of XCH_4 over this area. Mitsch et al. (2010) and Jauhiainen et al. (2005) both investigated the influence of water table depth on methane emissions from tropical wetlands. They both found decreasing methane emissions with increasing water table depths. Jauhiainen et al. (2005) also found that waterlogged conditions that are formed in the wet season can last for a relatively long period, possibly until the start of the dry season. So it is well possible that the wetlands in the Orinoco region were not yet fully dry in January 2019, still emitting

significant amounts of methane. The study by Mitsch et al. (2010) also showed that when the soils are too wet, they emit less methane, thus implying some optimum moisture conditions in between a minimum and maximum for which maximum CH_4 emissions occur. This might explain the observed difference in XCH_4 between January and August measured by TROPOMI, where the measured XCH_4 was higher in January than in August. It is possible that during the wet season in August, there was too much water in the soils of the wetlands, which limited the methane emissions by limited diffusion. During the dry season in January, when the soil is drier, but still sufficiently wet to trigger methane production, the methane emissions from these wetlands are not limited by too much water. So they are still emitting substantial amounts of methane and more compared to the August emissions.

4.1.3 Simulations with different fuel exploitation emissions

The hypothesis that fossil fuel emissions of methane are underestimated by EDGAR v4.3.2 playing an important role in the observed enhancement of XCH_4 by TROPOMI, as discussed in Section 4.1.1 and 4.1.2, is further tested. The fossil fuel methane emissions from EDGAR have been replaced by a different fossil fuel methane emission inventory. The fossil fuel methane emission inventory that is used is from Scarpelli et al. (2018). This emission inventory is based on reported emissions of each country to the United Nations Framework Convention on Climate Change (UNFCCC) in 2012, which is the same year as the EDGAR inventory. The difference between the fossil fuel emissions by EDGAR v4.3.2 and Scarpelli et al. (2018) is shown in Figure A.3 in the Appendix. The most important differences are found around Lake Maracaibo in the west of Venezuela and at the northeastern corner of the domain. So we expect to see the largest differences in those areas. Especially around Lake Maracaibo, the emissions of methane in the inventory by Scarpelli et al. (2018) are a lot higher.

Figure 11 and 12 show the results of the simulations where the fuel exploitation emissions from EDGAR are replaced by the emission inventory from Scarpelli et al. (2018). The fuel exploitation emission inventory from Scarpelli et al. (2018) does not significantly improve the result. Eventhough this emission inventory prescribes higher methane emissions for the model simulations, the effect on the resulting simulated enhancement in XCH_4 is relatively small. The largest differences between the simulations with fuel exploitation emissions by EDGAR and by Scarpelli et al. (2018) are as expected found around Lake Maracaibo. At this location Scarpelli et al. (2018) prescribe emissions that are much larger than EDGAR, where almost no emissions are present in this area. Unfortunately this area is not present in the TROPOMI measurements in January, so the effect of the enhanced emissions can not be compared with TROPOMI. In August however, the area around Lake Maracaibo is included in the TROPOMI measurements. Since measurements over large water bodies are removed, there is no data available directly above the lake. However, the WRF simulations show high mixing ratios of XCH_4 around Lake Maracaibo in Figure 11b. The simulated XCH_4 at this location is reasonably similar compared to TROPOMI, but this improved agreement between the WRF simulated and TROPOMI observed XCH_4 is only confined to a small area around these sources.

Another location where the simulated XCH_4 is slightly higher after implementing the emissions from Scarpelli et al. (2018), is at the Magdalena river valley. Eventhough the difference is small and hardly visible in Figures 11 and 12, it brings the WRF simulated XCH_4 closer to the measurements by TROPOMI in both seasons.

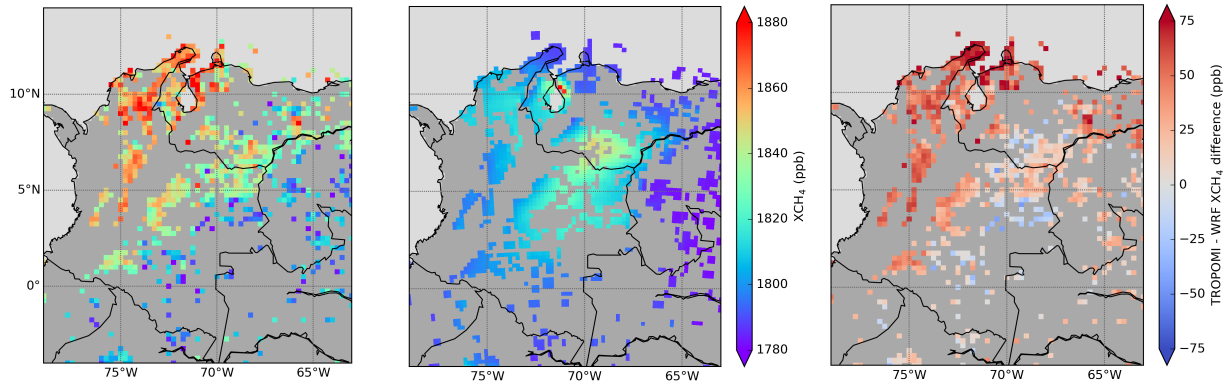

(a) TROPOMI **(b)** WRF **(c)** Difference

Figure 11 | Difference between TROPOMI and WRF for August with fuel exploitation emissions by Scarpelli et al. (2018). Column-average mixing ratios of CH_4 in August 2018, measured by TROPOMI (a) and simulated in WRF (b). Figure (c) shows the difference between TROPOMI and WRF, where red values indicate higher values for TROPOMI and blue values indicate higher values for WRF. The WRF data is filtered to only show the locations that are available in TROPOMI.

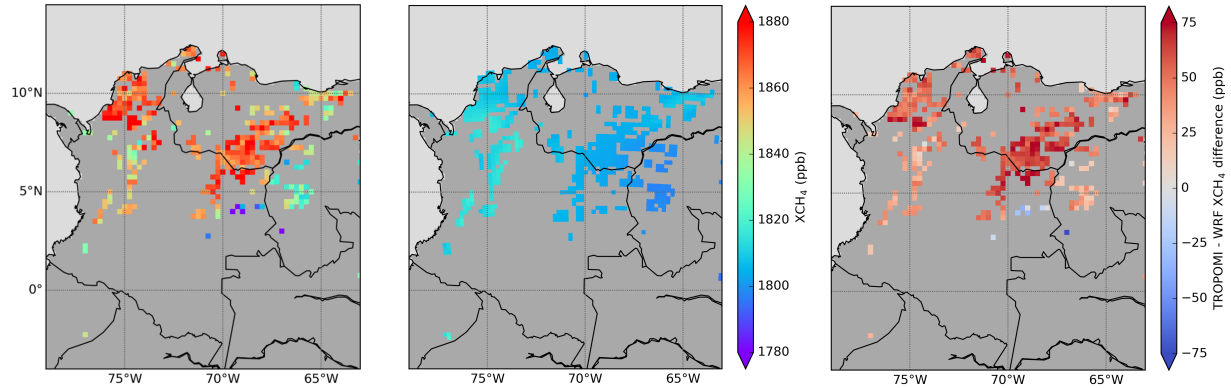

(a) TROPOMI **(b)** WRF **(c)** Difference

Figure 12 | Difference between TROPOMI and WRF for January with fuel exploitation emissions by Scarpelli et al. (2018). Column-average mixing ratios of CH_4 in January 2019, measured by TROPOMI (a) and simulated in WRF (b). Figure (c) shows the difference between TROPOMI and WRF, where red values indicate higher values for TROPOMI and blue values indicate higher values for WRF. The WRF data is filtered to only show the locations that are available in TROPOMI.

The results from the simulations with the fuel exploitation emissions by Scarpelli et al. (2018) indicate that a different fuel emission inventory does only partly reduce some of the differences that were observed. Especially the area around Lake Maracaibo saw an improvement. The maximum values that are simulated come close to what is measured by TROPOMI, but the extend of the area of the enhancement is still too small. Other emission sources are still needed to match the enhancement in XCH_4 that is observed by TROPOMI over northern Colombia.

4.1.4 Simulations with estimated missing emissions

With the information about the effect of CH_4 emissions on the resulting XCH_4, it can be estimated how much emissions are missing in the initial simulations using a simple column mass-balance approach (so assuming that all the missing methane in a vertical column originates at the surface of that column and is not supplied by advection). Based on the XCH_4 measurements from TROPOMI in August, an emission field is created with the fluxes that are needed to match these TROPOMI measurements. Subsequently, we have conducted an additional run in which we applied this inferred estimated emission field in WRF. The resulting XCH_4 from this simulation should be reasonably similar to the observations from TROPOMI. The comparison between this simulation and the TROPOMI observations will also provide more insight into the role of transport on XCH_4 and, consequently, the locations where the followed column mass-balance approach to infer missing emissions is not valid.

The calculated emission field is shown in Figure 13. The strongest emissions are found in the northern part of Colombia, around the Magdalena river basin, Guajira and around Lake Maracaibo. Methane emissions of $\sim 5.0 \times 10^{-9}$ kg/m^2/s are found in these areas. Since the Orinoco region was already represented well in the initial simulations, the methane emissions did not change much there. The methane emissions here are still $\sim 2.0 \times 10^{-9}$ kg/m^2/s.

The outcome of the simulation with the estimated emissions that are needed to match the XCH_4 that is measured by TROPOMI is visible in Figure 14. The agreement between the simulation and the measurements is obviously much better than before. Especially the Magdalena region in northwest Colombia is represented very well. Note, however, that the emissions that are needed to get this enhancement are around 5.0×10^{-9} kg/m^2/s, which is 10 times larger than the total surface CH_4 emission flux of 0.5×10^{-9} kg/m^2/s that was previously used in this area.

Also the area around Lake Maracaibo in Venezuela has improved significantly compared to previous simulations. The first simulation (Figure 9) showed no enhancement in this area, while the simulation with fuel emissions by Scarpelli et al. (2018) (Figure 11) resulted in an enhancement that was similar in magnitude, but not in size. After the estimation of the emissions that are needed to match XCH_4 measured by TROPOMI, the enhancement of XCH_4 is similar in size and magnitude.

The most striking difference that is still visible, is at the northern peninsula of Colombia, the Guajira region. Eventhough large methane emissions are implemented in this region, still no enhancement in XCH_4

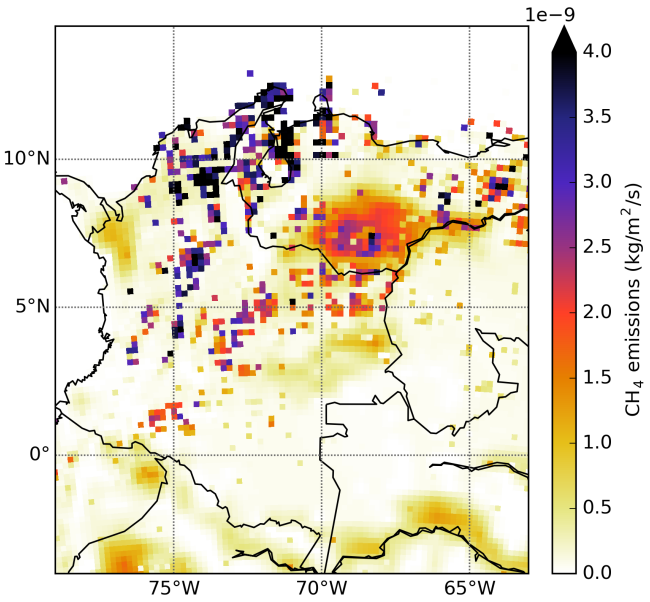

Figure 13 | Estimated CH_4 emissions to match TROPOMI. Estimated CH_4 emissions in $kg/m^2/s$ for August to match XCH_4 measurements by TROPOMI.

is present. This is also pointing out the important role of transport in this region, also reflected by the strong winds that are present in this area, which transports the emitted CH_4 in a southwestern direction. At the locations where a high enhancement is present there is almost no wind, so the emitted CH_4 is not transported, but stays at the same place for a longer time. These wind patterns are visible in Figure A.4 in the appendix.

An other interesting pattern that becomes visible with this simulation, is the role of orography. In Figure A.4 in the appendix, the terrain height is plotted jointly with the simulated XCH_4. It is clearly visible that the emitted CH_4 seems to be mostly confined to the lower elevated areas. Especially over the Magdalena region, which is surrounded by mountains at the east and south, the role of orography is very strong. The mountains seem to block the transport of methane towards the east and south, which causes the methane to accumulate over the Magdalena region.

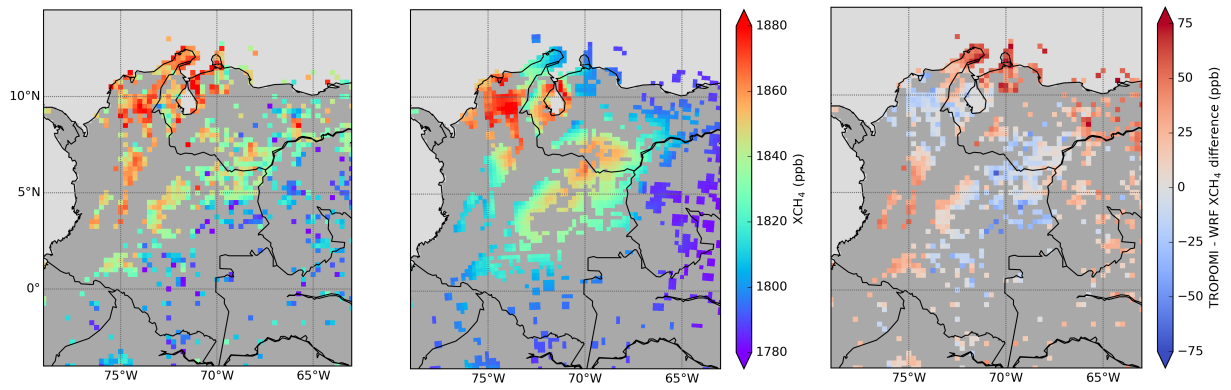

(a) TROPOMI **(b)** WRF **(c)** Difference

Figure 14 | Difference between TROPOMI and WRF for August with estimated emissions to match TROPOMI. Column-average mixing ratios of CH_4 in August 2018, measured by TROPOMI (a) and simulated in WRF (b). Figure (c) shows the difference between TROPOMI and WRF, where red values indicate higher values for TROPOMI and blue values indicate higher values for WRF. The WRF data is filtered to only show the locations that are available in TROPOMI.

4.2 Limitations and Recommendations

4.2.1 Inundation data

The inundation data used to compare with wetland CH_4 emissions in Figure 6, have been measured in the period between 2007 and 2011. The wetland CH_4 emissions from the LPX inventory that are shown in the same figure are based on the year 2012. This slight mismatch in years might cause little differences, since the meteorological conditions might be different, especially regarding the important role of ENSO events in this region. In addition, the inundation data from Quiñones et al. (2016) is originally measured at a resolution of 100 $\times$ 100 meters, but have been converted for the presented study, also for practical reasons, to a resolution of 0.05 $\times$ 0.05 degrees. The wetland emission inventory has a much coarser resolution of 0.5 $\times$ 0.5 degrees. Regarding this large difference in spatial resolution, it is interesting to further investigate in a more quantitative manner the actual area of wetlands present within the LPX 0.5 $\times$ 0.5 degree grid boxes to identify potential misrepresentations of wetland area in LPX.

4.2.2 Anthropogenic CH_4 emissions

The simulation performed during this thesis with only the EDGAR v4.3.2 database as an input of anthropogenic CH_4 emissions, did not reproduce the XCH_4 mixing ratios observed by TROPOMI very well in both the dry and wet season. We expect that the differences in XCH_4 between the WRF simulations and TROPOMI are partly caused by an underestimation of CH_4 emissions by fuel exploitation in EDGAR. This hypothesis is in line with several other studies, which also found an underestimation of methane emissions

from fossil fuel extraction by EDGAR (Miller et al., 2013; Maasakkers et al., 2019). For future research that includes methane emissions, we recommend to not only rely on the EDGAR database, but also use other fuel exploitation emission inventories.

We also need to carefully consider the reference years of both the EDGAR v4.3.2 and Scarpelli methane emission inventories, which is 2012 for both. Given that since 2012, there are potentially fast changes in the fossil fuel production industry, especially in Venezuela as a result of the recent societal-economical developments. It might be that some of the TROPOMI observed strong enhancements in XCH_4 over northern Colombia and parts of Venezuela might point at some large sources of methane associated with a leaky production process, also due to stalled maintenance.

Another disadvantage of the EDGAR emission database, is that this data comes as a yearly average. Because of this, the seasonal variability of anthropogenic emissions of methane is not captured. For this thesis, the anthropogenic emissions are assumed to be equal in January and August.

4.2.3 Wetland CH_4 emissions

The wetland CH_4 emission inventory from LPX that is used for the simulations in this thesis is based on monthly averaged emission rates of 2012. For the purpose of this thesis, where we were interested to make a first-order assessment of the role of different CH_4 sources in remote-sensing based enhanced XCH_4 over Colombia, application of these LPX data seems to be sufficient. However, also now having established that there seems to be inconsistencies regarding the seasonal contrasts between the TROPOMI observed- and WRF simulated XCH_4 over regions where these wetland emissions dominate, it might be useful to implement wetland CH_4 emissions as a function of properties that influence the emission rate, like precipitation and soil moisture (Walter and Heimann, 2000). Important to keep in mind when implementing such a model is that it can become computationally costly.

As has been shown and discussed in Section 3.2, there are particular mismatches between the wetland CH_4 emissions from LPX and inundation conditions. Especially in the regions where high inundation conditions are measured in combination with high XCH_4 measured by TROPOMI, it is likely that LPX underestimates some of the wetland emissions. Therefore it would be interesting for future research to compare the LPX emissions with other wetland CH_4 emission inventories, like the data from Bloom et al. (2017).

4.2.4 WRF simulations

The meteorological output of WRF simulations has not been extensively evaluated in this study by comparison with in-situ measurements. However, Koetsenruijter (2017) did validate the WRF model elaborately for Colombia. He used the same boundary conditions from ECMWF, a similar domain and the same parameterization schemes for the most important parameters. He evaluated the output of the model simulations with 5 measurement stations in Colombia for surface temperature, water mixing ratio and wind speed. This evaluation of the WRF simulated meteorology for the study domain showed a reasonable agreement

between the WRF model and in-situ measurements.

The WRF simulations are performed with initial and boundary conditions by CAMS for methane. This data is fairly accurate for background mixing ratios of CH_4, but in areas which are affected by regional emissions, the simulation of the spatial and temporal variability is less accurate (Koffi and Bergamaschi, 2018). The lack of spatial variability in the CAMS data causes an initial condition of the domain that has little spread. The initial methane mixing ratios for the WRF simulations range between 1800 and 1820 ppb for the entire column up to 100 hPa, while the XCH_4 measured by TROPOMI has a much larger spread, between 1780 and 1880 ppb. Therefore, maximum surface methane mixing ratios of 1820 ppb seem a bit low. Ideally we want to use the TROPOMI measurements itself as initial and boundary conditions, but due to insufficient coverage this is not possible yet. When TROPOMI would provide a full coverage of the domain and surroundings, we could use this data to provide the boundary conditions for the WRF simulations on these XCH_4 enhancement analyses.

The maximum height of the WRF domain is 100 hPa, while the maximum height of the TROPOMI measurements is 0.1 hPa. Therefore we corrected the WRF calculated XCH_4 to consider this contribution to the XCH_4 up to 0.1 hPa assuming a typically observed CH_4 mixing ratio profile for this part of the domain (see Section 2.5).

For the calculation of the column average mixing ratio of CH_4 from WRF, we did not apply the column averaging kernel from TROPOMI. However, ignoring this TROPOMI averaging kernel is also justified given that the averaging kernel is close to 1 for the lower atmosphere (see Figure A.5 in the Appendix). This implies that the WRF simulated XCH_4 after applying the averaging kernel will only change by a few percent, not affecting the overall conclusions on the substantial misrepresentation of CH_4 emissions in WRF. However, for follow-up studies, where our main priority would be to get especially an improved coverage of the TROPOMI observations, should indeed apply this averaging kernel. Figure A.5 shows that the averaging kernel is at its maximum at approximately 10 km altitude with already quite reduced CH_4 mixing ratios compared to the lower troposphere and the boundary layer. This implies that actual application of the averaging kernel would probably further reduce the WRF calculated XCH_4.

Another limitation of the WRF simulations in this thesis is the years that are used. The different datasets and inventories are not all from the same year. The GFED data is from 2014 and the EDGAR data is from 2012, while the LPX inventory is also based on 2012. The meteorological and chemical boundary conditions that are applied to the simulations are from respectively 2014 and 2018. For the main purpose of this thesis study, the mismatch between the reference years of the different components included in the followed research approach was not deemed to pose a main limiting factor, since the conducted analysis has provided a first-order insight in the role and representation of the different CH_4 sources in the study domain. It is, however, important to have recent boundary conditions for the CH_4 mixing ratios, since these mixing ratios increase quite rapidly, up to 10 ppb/year in recent years (Dlugokencky, 2019). It would of course be best to have all the data from the same year as the measurements by TROPOMI. Unfortunately for this thesis this

was not possible, since the most recent data were not available.

The last thing to note about the simulations performed by WRF is that methane is implemented as a passive tracer. This means that there are no chemical reactions taking place, while in the atmosphere oxidation by OH is the primary sink of methane (Rigby et al., 2017). Because of this, there is no loss of methane included in the simulations. Since the lifetime of methane is relatively long compared to the duration of the simulation (9 years vs. 1 month), but more importantly, given the residence time of methane in the study domain on the order of some days, it will not have a big impact on the results.

4.2.5 TROPOMI

The largest limitation of the TROPOMI XCH_4 data is the poor coverage. Due to a very strict filter for clouds and other properties, few data points remain. Because of this limited coverage it is not possible to compare the WRF simulated XCH_4 for all regions. Unfortunately some interesting regions are missing in both the January and August TROPOMI data, like the Chocó region. This region is known for its heavy rainfall almost all year long and, consequently, a potential large source of CH_4, but which cannot easily be retrieved from the TROPOMI data due to the high cloud cover. An other region that is not present in both datasets is the Amazon. Just like the Chocó region this would have been an interesting area to include in the analysis. Recommended for other studies in the future with methane measurements by TROPOMI is to apply a less strict filter to the TROPOMI data. A disadvantage is that it will be more costly to process the data and that the data might be less accurate. But at least potentially revealing some insights in the sources from the vast tropical rainforests of Colombia and neighboring countries.

For this thesis, we only have the TROPOMI monthly averaged XCH_4 data over the area around Colombia available for several months. This data is compared to a 2-year average of the entire Earth measured by SCIAMACHY to compare the magnitude and distribution of the XCH_4 enhancement. To make the best possible comparison and to be sure that there is an enhancement visible like was observed with SCIAMACHY, we ideally want to have a similar processing of the data. This would mean that we want a yearly average of the XCH_4 measured by TROPOMI for the entire earth. Another advantage of taking a yearly average in stead of a monthly average is that most likely the coverage will increase.

In the comparison between the WRF simulated XCH_4 and the measured XCH_4 by TROPOMI, the data from TROPOMI is used as a true value. Since methane observations from TROPOMI are relatively new and not well studied yet, it needs though to be more extensively validated. However, a first comparison between TROPOMI and GOSAT shows a good agreement (Hu et al., 2018), and which provides confidence in these TROPOMI data as a good reference for the potential large enhancement in XCH_4 over Colombia due to some of the identified, potentially large sources.

5 Conclusion

The aim of this study was to compare new TROPOMI satellite measurements of methane over Colombia with model simulations performed in WRF. First the TROPOMI measurements are compared with older observations by SCIAMACHY to see if a similar enhancement is visible. Next, we investigated how model simulations considering state-of-the-art global emission inventories for biomass burning, anthropogenic and wetland emissions compare to observations from TROPOMI. The seasonal variability of the atmospheric methane and the influence of natural sources was investigated by comparing the dry season (January) with the wet season (August). Lastly, the influence of a different inventory for fossil fuel exploitation emissions was investigated and the remaining missing methane emissions are estimated.

The first conclusion we can draw from the presented analysis, is that the TROPOMI observations show that there is still a significant enhancement of XCH_4 present over Colombia. Compared to previous observations made by SCIAMACHY in the early 2000s, a similar magnitude and extend of the enhancement can be seen. The enhanced XCH_4 covers large parts of Colombia, including the Andes mountains, the Orinoco River Basin and the Magdalena River Valley. High values are also observed around Lake Maracaibo in Venezuela. Peak values of more than 1880 ppb are found in the northwestern part of Colombia and close to Lake Maracaibo. Compared to background values of 1780 ppb at the southern half of Colombia, this is an enhancement of $\sim$100 ppb. An other interesting outcome of the comparison between TROPOMI measurements and SCIAMACHY measurements, which were collected $\sim$15 years ago, is that the absolute XCH_4 has increased by over 100 ppb in those 15 years, which is an increase of about 6%.

The simulations with WRF-Chem, using only biomass burning, anthropogenic and wetland emissions were not able to reproduce the measurements from TROPOMI very well. Large differences were observed over northwestern Colombia in both August and January, where differences between the TROPOMI observed and WRF simulated XCH_4 of over 75 ppb are observed. Most likely the reason of this underestimation is reflecting a combination of underestimations of the different CH_4 sources in this region. This area showed a high inundation density in both January and August, but little methane emissions from wetlands in both seasons. So it is likely that the wetland emissions are underestimated. This part of the country is also a known location of palm oil production, which is known to emit methane. This could possibly be another explanation for the discrepancy between the observed and simulated XCH_4, but it must be further investigated which agricultural emissions are actually considered in the EDGAR emissions inventory.

Over the Orinoco region, the simulation of August showed a reasonable agreement with TROPOMI. This is a region with large emissions due to wetlands. A striking result was observed in January, where a large enhancement in XCH_4 was observed over the Orinoco region by TROPOMI, but not simulated by WRF. We did not expect to find high methane mixing ratios in this region, because of the anticipated seasonal cycle in methane emissions by wetlands. This would result in strongly reduced CH_4 emissions, because of the prevailing dry conditions for this region in January. A possible explanation is that the methane

emissions from biomass burning are underestimated, but since the contribution of biomass burning to the total methane budget is very small compared to other sources, it is not likely that this can cause such a high enhancement. A different possibility is that wetlands keep emitting methane, even if it is the dry season. The waterlogged conditions that were formed during the wet season, may still be present in January.

The influence of uncertainties in methane sources associated with fossil fuel exploitation has been investigated by changing the fuel exploitation emissions from EDGAR with the inventory by Scarpelli et al. (2018). This resulted in a better agreement between the WRF simulated and TROPOMI observed XCH_4 around Lake Maracaibo. However, the overall performance of the simulations, taking the whole domain into account, did not significantly improve.

From the XCH_4 measured by TROPOMI in August, the methane emissions that are needed to match these measurements was calculated. Simulations with these estimated emissions showed that methane emissions over northwest Colombia have to increase by a factor 10 compared to the inventories to match TROPOMI observed XCH_4.

Overall, this study showed that there is still an enhancement of XCH_4 over Colombia, but it remains very uncertain what causes this. The Magdalena region in north-west Colombia shows elevated XCH_4 in the TROPOMI observations in both the dry and wet season, which are not simulated by WRF. This is likely caused by an underestimation of emissions by wetlands and agriculture in this area. High values of XCH_4 are observed over the Orinoco wetland regions during the dry season, when there are no emissions expected. Wetland emissions during dry season are a possibility to cause an enhancement of the magnitude that is observed, but this is very uncertain. So more research is needed to investigate where this methane comes from.

References

Allen, D. T., Torres, V. M., Thomas, J., Sullivan, D. W., Harrison, M., Hendler, A., Herndon, S. C., Kolb, C. E., Fraser, M. P., Hill, A. D., et al. (2013). Measurements of methane emissions at natural gas production sites in the United States. *Proceedings of the National Academy of Sciences*, 110(44):17768–17773.

Archer, D., Eby, M., Brovkin, V., Ridgwell, A., Cao, L., Mikolajewicz, U., Caldeira, K., Matsumoto, K., Munhoven, G., Montenegro, A., et al. (2009). Atmospheric lifetime of fossil fuel carbon dioxide. *Annual review of earth and planetary sciences*, 37:117–134.

Armenteras, D., Rodríguez, N., Retana, J., and Morales, M. (2011). Understanding deforestation in montane and lowland forests of the colombian andes. *Regional Environmental Change*, 11(3):693–705.

Betts, A. K. (1986). A new convective adjustment scheme. part i: Observational and theoretical basis. *Quarterly Journal of the Royal Meteorological Society*, 112(473):677–691.

Bloom, A. A., Bowman, K. W., Lee, M., Turner, A. J., Schroeder, R., Worden, J. R., Weidner, R., McDonald, K. C., and Jacob, D. J. (2017). A global wetland methane emissions and uncertainty dataset for atmospheric chemical transport models (WetCHARTs version 1.0). *Geoscientific Model Development*, 10(6):2141–2156.

Bousquet, P., Ciais, P., Miller, J. B., Dlugokencky, E. J., Hauglustaine, D. A., Prigent, C., Van der Werf, G. R., Peylin, P., Brunke, E.-G., Carouge, C., Langenfelds, R. L., Lathière, J., Papa, F., Ramonet, M., Schmidt, M., Steele, L. P., Tyler, S. C., and White, J. (2006). Contribution of anthropogenic and natural sources to atmospheric methane variability. *Nature*, 443(7110):439–443.

Bovensmann, H., Burrows, J., Buchwitz, M., Frerick, J., Noël, S., Rozanov, V., Chance, K., and Goede, A. (1999). Sciamachy: Mission objectives and measurement modes. *Journal of the atmospheric sciences*, 56(2):127–150.

Butz, A., Galli, A., Hasekamp, O., Landgraf, J., Tol, P., and Aben, I. (2012). Tropomi aboard sentinel-5 precursor: Prospective performance of ch4 retrievals for aerosol and cirrus loaded atmospheres. *Remote sensing of environment*, 120:267–276.

Butz, A., Hasekamp, O., Frankenberg, C., Vidot, J., and Aben, I. (2010). Ch4 retrievals from space-based solar backscatter measurements: Performance evaluation against simulated aerosol and cirrus loaded scenes. *Journal of Geophysical Research: Atmospheres*, 115(D24).

Chanton, J. P. and Smith, L. K. (1993). Seasonal variations in the isotopic composition of methane associated with aquatic macrophytes. In *Biogeochemistry of Global Change*, pages 619–632. Springer.

Chen, F. and Dudhia, J. (2001). Coupling an advanced land surface–hydrology model with the penn state–ncar mm5 modeling system. part i: Model implementation and sensitivity. *Monthly Weather Review*, 129(4):569–585.

Christensen, T. R., Ekberg, A., Ström, L., Mastepanov, M., Panikov, N., Öquist, M., Svensson, B. H., Nykänen, H., Martikainen, P. J., and Oskarsson, H. (2003). Factors controlling large scale variations in methane emissions from wetlands. *Geophysical Research Letters*, 30(7).

Couwenberg, J., Dommain, R., and Joosten, H. (2010). Greenhouse gas fluxes from tropical peatlands in south-east asia. *Global Change Biology*, 16(6):1715–1732.

Crippa, M., Guizzardi, D., Muntean, M., Schaaf, E., Dentener, F., van Aardenne, J. A., Monni, S., Doering, U., Olivier, J. G., Pagliari, V., et al. (2018). Gridded emissions of air pollutants for the period 1970–2012 within EDGAR v4. 3.2. *Earth System Science Data*, 10(4):1987–2013.

Dlugokencky, E. J. (2019). Trends in Atmospheric Methane (www.esrl.noaa.gov/gmd/ccgg/trends_ch4/). *NOAA/ESRL*.

Dlugokencky, E. J., Houweling, S., Bruhwiler, L., Masarie, K. A., Lang, P. M., Miller, J. B., and Tans, P. P. (2003). Atmospheric methane levels off: Temporary pause or a new steady-state? *Geophysical Research Letters*, 30(19):1992.

Dudhia, J. (1989). Numerical study of convection observed during the winter monsoon experiment using a mesoscale two-dimensional model. *Journal of the atmospheric sciences*, 46(20):3077–3107.

Duncan, B. N., Martin, R. V., Staudt, A. C., Yevich, R., and Logan, J. A. (2003). Interannual and seasonal variability of biomass burning emissions constrained by satellite observations. *Journal of Geophysical Research: Atmospheres*, 108(D2):ACH–1.

FAO (2018). 2018/19 El Niño: High risk countries and potential impacts on food security and agriculture. *Food and Agriculture Organization of the United Nations*.

Forster, P., Ramaswamy, V., Artaxo, P., Berntsen, T., Betts, R., Fahey, D., Haywood, J., Lean, J., Lowe, D., Myhre, G., Nganga, J., Prinn, R., Raga, G., Schulz, M., and Van Dorland, R. (2007). *Climate change 2007 : the physical science basis : contribution of Working Group I to the Fourth Assessment Report of the Intergovernmental Panel on Climate Change*. Cambridge University Press.

Frankenberg, C., Bergamaschi, P., Butz, A., Houweling, S., Meirink, J. F., Notholt, J., Petersen, A. K., Schrijver, H., Warneke, T., and Aben, I. (2008). Tropical methane emissions: A revised view from SCIAMACHY onboard ENVISAT. *Geophysical Research Letters*, 35(15):L15811.

Frankenberg, C., Meirink, J. F., Bergamaschi, P., Goede, A. P. H., Heimann, M., Körner, S., Platt, U., van Weele, M., and Wagner, T. (2006). Satellite chartography of atmospheric methane from SCIAMACHY on board ENVISAT: Analysis of the years 2003 and 2004. *Journal of Geophysical Research*, 111(D7):D07303.

Frankenberg, C., Meirink, J. F., van Weele, M., Platt, U., and Wagner, T. (2005). Assessing methane emissions from global space-borne observations. *Science*, 308(5724):1010–1014.

Giglio, L., Randerson, J. T., and van der Werf, G. R. (2013). Analysis of daily, monthly, and annual burned area using the fourth-generation global fire emissions database (GFED4). *Journal of Geophysical Research: Biogeosciences*, 118(1):317–328.

Grell, G. A., Peckham, S. E., Schmitz, R., McKeen, S. A., Frost, G., Skamarock, W. C., and Eder, B. (2005). Fully coupled "online" chemistry within the WRF model. *Atmospheric Environment*, 39(37):6957–6975.

Hansen, J. E. and Sato, M. (2001). Trends of measured climate forcing agents. *Proceedings of the National Academy of Sciences*, 98(26):14778–14783.

Hariprasad, K., Srinivas, C., Singh, A. B., Rao, S. V. B., Baskaran, R., and Venkatraman, B. (2014). Numerical simulation and intercomparison of boundary layer structure with different PBL schemes in WRF using experimental observations at a tropical site. *Atmospheric Research*, 145:27–44.

Hasekamp, O., Lorente, A., Hu, H., Butz, A., Aan de Brugh, J., and Landgraf, J. (2019). Algorithm Theoretical Baseline Document for Sentinel-5 Precursor Methane Retrieval. *SRON*.

Hong, S.-Y., Noh, Y., and Dudhia, J. (2006). A new vertical diffusion package with an explicit treatment of entrainment processes. *Monthly weather review*, 134(9):2318–2341.

Hu, H., Hasekamp, O., Butz, A., Galli, A., Landgraf, J., Aan de Brugh, J., Borsdorff, T., Scheepmaker, R., and Aben, I. (2016). The operational methane retrieval algorithm for TROPOMI. *Atmospheric Measurement Techniques*, 9(11):5423–5440.

Hu, H., Landgraf, J., Detmers, R., Borsdorff, T., Aan de Brugh, J., Aben, I., Butz, A., and Hasekamp, O. (2018). Toward Global Mapping of Methane With TROPOMI: First Results and Intersatellite Comparison to GOSAT. *Geophysical Research Letters*, 45(8):3682–3689.

Hu, X.-M., Nielsen-Gammon, J. W., Zhang, F., Hu, X.-M., Nielsen-Gammon, J. W., and Zhang, F. (2010). Evaluation of Three Planetary Boundary Layer Schemes in the WRF Model. *Journal of Applied Meteorology and Climatology*, 49(9):1831–1844.

IPCC (2006). 2006 IPCC guidelines for national greenhouse gas inventories.

Janssens-Maenhout, G., Crippa, M., Guizzardi, D., Muntean, M., Schaaf, E., Dentener, F., Bergamaschi, P., Pagliari, V., Olivier, J. G. J., Peters, J. A. H. W., van Aardenne, J. A., Monni, S., Doering, U., and Petrescu, A. M. R. (2017). EDGAR v4.3.2 Global Atlas of the three major Greenhouse Gas Emissions for the period 1970–2012. *Earth System Science Data Discussions*, 2017:1–55.

Jauhiainen, J., Takahashi, H., Heikkinen, J. E., Martikainen, P. J., and Vasander, H. (2005). Carbon fluxes from a tropical peat swamp forest floor. *Global Change Biology*, 11(10):1788–1797.

Kenea, S. T., Oh, Y.-S., Goo, T.-Y., Rhee, J.-S., Byun, Y.-H., Labzovskii, L. D., and Li, S. (2019). Comparison of XCH 4 Derived from gb FTS and GOSAT and Evaluation Using Aircraft In-Situ Observations over TCCON Site. *Asia-Pacific Journal of Atmospheric Sciences*, pages 1–13.

Keppler, F., Hamilton, J. T. G., Braß, M., and Röckmann, T. (2006). Methane emissions from terrestrial plants under aerobic conditions. *Nature*, 439(7073):187–191.

Kirschke, S., Bousquet, P., Ciais, P., Saunois, M., Canadell, J. G., Dlugokencky, E. J., Bergamaschi, P., Bergmann, D., Blake, D. R., Bruhwiler, L., Cameron-Smith, P., Castaldi, S., Chevallier, F., Feng, L., Fraser, A., Heimann, M., Hodson, E. L., Houweling, S., Josse, B., Fraser, P. J., Krummel, P. B., Lamarque, J.-F., Langenfelds, R. L., Le Quéré, C., Naik, V., O'Doherty, S., Palmer, P. I., Pison, I., Plummer, D., Poulter, B., Prinn, R. G., Rigby, M., Ringeval, B., Santini, M., Schmidt, M., Shindell, D. T., Simpson, I. J., Spahni, R., Steele, L. P., Strode, S. A., Sudo, K., Szopa, S., van der Werf, G. R., Voulgarakis, A., van Weele, M., Weiss, R. F., Williams, J. E., and Zeng, G. (2013). Three decades of global methane sources and sinks. *Nature Geoscience*, 6(10):813–823.

Koetsenruijter, G. (2017). Modelling the meteorological impacts of future land use change in Colombian Orinoco. *Wageningen University & Research*.

Koffi, E. and Bergamaschi, P. (2018). *Evaluation of Copernicus Atmosphere Monitoring Service methane products*. Joint Research Centre.

Lelieveld, J., Crutzen, P. J., and Dentener, F. J. (1998). Changing concentration, lifetime and climate forcing of atmospheric methane. *Tellus B*, 50(2):128–150.

Maasakkers, J. D., Jacob, D. J., Sulprizio, M. P., Scarpelli, T. R., Nesser, H., Sheng, J.-X., Zhang, Y., Hersher, M., Bloom, A. A., Bowman, K. W., et al. (2019). Global distribution of methane emissions, emission trends, and OH concentrations and trends inferred from an inversion of GOSAT satellite data for 2010–2015. *Atmospheric Chemistry and Physics*, 19(11):7859–7881.

Maclean, J., Hardy, B., and Hettel, G. (2013). *Rice Almanac: Source book for one of the most important economic activities on earth*. IRRI.

Massart, S., Agusti-Panareda, A., Aben, I., Butz, A., Chevallier, F., Crevoisier, C., Engelen, R., Frankenberg, C., and Hasekamp, O. (2014). Assimilation of atmospheric methane products in the macc-ii system: from sciamachy to tanso and iasi. *Atmospheric Chemistry and Physics*, 14.

Miller, S. M., Wofsy, S. C., Michalak, A. M., Kort, E. A., Andrews, A. E., Biraud, S. C., Dlugokencky, E. J., Eluszkiewicz, J., Fischer, M. L., Janssens-Maenhout, G., et al. (2013). Anthropogenic emissions of methane in the United States. *Proceedings of the National Academy of Sciences*, 110(50):20018–20022.

Mitsch, W. J., Nahlik, A., Wolski, P., Bernal, B., Zhang, L., and Ramberg, L. (2010). Tropical wetlands: seasonal hydrologic pulsing, carbon sequestration, and methane emissions. *Wetlands ecology and management*, 18(5):573–586.

Mlawer, E. J., Taubman, S. J., Brown, P. D., Iacono, M. J., and Clough, S. A. (1997). Radiative transfer for inhomogeneous atmospheres: RRTM, a validated correlated-k model for the longwave. *Journal of Geophysical Research: Atmospheres*, 102(D14):16663–16682.

Morrison, H., Thompson, G., and Tatarskii, V. (2009). Impact of cloud microphysics on the development of trailing stratiform precipitation in a simulated squall line: Comparison of one-and two-moment schemes. *Monthly Weather Review*, 137(3):991–1007.

Mullendore, G. L., Durran, D. R., and Holton, J. R. (2005). Cross-tropopause tracer transport in midlatitude convection. *Journal of Geophysical Research: Atmospheres*, 110(D6).

Neue, H., Gaunt, J., Wang, Z., Becker-Heidmann, P., and Quijano, C. (1997). Carbon in tropical wetlands. *Geoderma*, 79(1-4):163–185.

Nisbet, E. and Chappellaz, J. (2009). Shifting gear, quickly. *Science*, 324(5926):477–478.

Nisbet, E. G., Dlugokencky, E. J., and Bousquet, P. (2014). Methane on the rise—again. *Science*, 343(6170):493–495.

Nisbet, E. G., Dlugokencky, E. J., Manning, M. R., Lowry, D., Fisher, R. E., France, J. L., Michel, S. E., Miller, J. B., White, J. W. C., Vaughn, B., Bousquet, P., Pyle, J. A., Warwick, N. J., Cain, M., Brownlow, R., Zazzeri, G., Lanoisellé, M., Manning, A. C., Gloor, E., Worthy, D. E. J., Brunke, E.-G., Labuschagne, C., Wolff, E. W., and Ganesan, A. L. (2016). Rising atmospheric methane: 2007-2014 growth and isotopic shift. *Global Biogeochemical Cycles*, 30(9):1356–1370.

Pandey, S., Houweling, S., Krol, M., Aben, I., Monteil, G., Nechita-Banda, N., Dlugokencky, E. J., Detmers, R., Hasekamp, O., Xu, X., Riley, W. J., Poulter, B., Zhang, Z., McDonald, K. C., White, J. W. C., Bousquet, P., and Röckmann, T. (2017). Enhanced methane emissions from tropical wetlands during the 2011 La Niña. *Scientific Reports*, 7(1):45759.

Petrenko, V. V., Smith, A. M., Brook, E. J., Lowe, D., Riedel, K., Brailsford, G., Hua, Q., Schaefer, H., Reeh, N., Weiss, R. F., et al. (2009). $^{14}CH_4$ measurements in Greenland ice: investigating last glacial termination CH_4 sources. *Science*, 324(5926):506–508.

Poveda, G. and Mesa, O. J. (2000). On the existence of lloró (the rainiest locality on earth): Enhanced ocean-land-atmosphere interaction by a low-level jet. *Geophysical research letters*, 27(11):1675–1678.

Quiñones, M., Vissers, M., Pacheco-Pascaza, A. M., Flórez, C., Estupiñán-Suárez, L. M., Aponte, C., Jaramillo Villa, U., Huertas, C., and Hoekman, D. (2016). Un enfoque ecosistémico para el análisis de una serie densa de tiempo de imágenes de radar alos palsar, para el mapeo de zonas inundadas en el territorio continental colombiano. *Biota Colombiana*, 17(1).

Reboredo, B., Arasa, R., and Codina, B. (2015). Evaluating sensitivity to different options and parameterizations of a coupled air quality modelling system over Bogotá, Colombia. Part I: WRF Model configuration. *Open Journal of Air Pollution*, 4(02):47.

Reijnders, L. and Huijbregts, M. (2008). Palm oil and the emission of carbon-based greenhouse gases. *Journal of cleaner production*, 16(4):477–482.

Rigby, M., Montzka, S. A., Prinn, R. G., White, J. W., Young, D., O'Doherty, S., Lunt, M. F., Ganesan, A. L., Manning, A. J., Simmonds, P. G., et al. (2017). Role of atmospheric oxidation in recent methane growth. *Proceedings of the National Academy of Sciences*, 114(21):5373–5377.

Rigby, M., Prinn, R. G., Fraser, P. J., Simmonds, P. G., Langenfelds, R. L., Huang, J., Cunnold, D. M., Steele, L. P., Krummel, P. B., Weiss, R. F., O'Doherty, S., Salameh, P. K., Wang, H. J., Harth, C. M., Mühle, J., and Porter, L. W. (2008). Renewed growth of atmospheric methane. *Geophysical Research Letters*, 35(22):L22805.

Ringeval, B., Houweling, S., Van Bodegom, P. M., Spahni, R., Van Beek, R., Joos, F., and Röckmann, T. (2014). Methane emissions from floodplains in the Amazon Basin: Challenges in developing a process-based model for global applications. *Biogeosciences*, 11(6):1519–1558.

Rosenqvist, A., Shimada, M., Ito, N., and Watanabe, M. (2007). ALOS PALSAR: A Pathfinder Mission for Global-Scale Monitoring of the Environment. *IEEE Transactions on Geoscience and Remote Sensing*, 45(11):3307–3316.

Scarpelli, T., Jacob, D., Maasakkers, J., Sheng, J. X., Rose, K., Payer Sulprizio, M., and Worden, J. (2018). A Global Gridded Inventory of Methane Emissions from Fuel Exploitation including Oil, Gas, and Coal. *AGU Fall Meeting Abstracts*.

Smith, L. K., Lewis, W. M., Chanton, J. P., Cronin, G., and Hamilton, S. K. (2000). Methane emissions from the Orinoco River floodplain, Venezuela. *Biogeochemistry*, 51(2):113–140.

Sugawara, S., Nakazawa, T., Shirakawa, Y., Kawamura, K., Aoki, S., Machida, T., and Honda, H. (1997). Vertical profile of the carbon isotopic ratio of stratospheric methane over Japan. *Geophysical research letters*, 24(23):2989–2992.

Turner, A. J., Frankenberg, C., Wennberg, P. O., and Jacob, D. J. (2017). Ambiguity in the causes for decadal trends in atmospheric methane and hydroxyl. *Proceedings of the National Academy of Sciences*, 114(21):5367–5372.

Van Beek, L. and Bierkens, M. F. (2009). The global hydrological model pcr-globwb: conceptualization, parameterization and verification. *Utrecht University, Utrecht, The Netherlands*, 1:25–26.

Walter, B. P. and Heimann, M. (2000). A process-based, climate-sensitive model to derive methane emissions from natural wetlands: Application to five wetland sites, sensitivity to model parameters, and climate. *Global Biogeochemical Cycles*, 14(3):745–765.

Wania, R., Ross, I., and Prentice, I. (2010). Implementation and evaluation of a new methane model within a dynamic global vegetation model: Lpj-whyme v1. 3.1. *Geoscientific Model Development*, 3(2):565–584.

Warmuzinski, K. (2008). Harnessing methane emissions from coal mining. *Process safety and environmental protection*, 86(5):315–320.

Yacob, S., Hassan, M. A., Shirai, Y., Wakisaka, M., and Subash, S. (2006). Baseline study of methane emission from anaerobic ponds of palm oil mill effluent treatment. *Science of the total environment*, 366(1):187–196.

Yokota, T., Yoshida, Y., Eguchi, N., Ota, Y., Tanaka, T., Watanabe, H., and Maksyutov, S. (2009). Global concentrations of co2 and ch4 retrieved from gosat: First preliminary results. *Sola*, 5:160–163.

Yu, Z., Loisel, J., Brosseau, D. P., Beilman, D. W., and Hunt, S. J. (2010). Global peatland dynamics since the last glacial maximum. *Geophysical Research Letters*, 37(13).

Appendix

Figure A.1 | **Distribution of peatlands.** Known locations of peatlands for the area around Colombia in green (Yu et al., 2010).

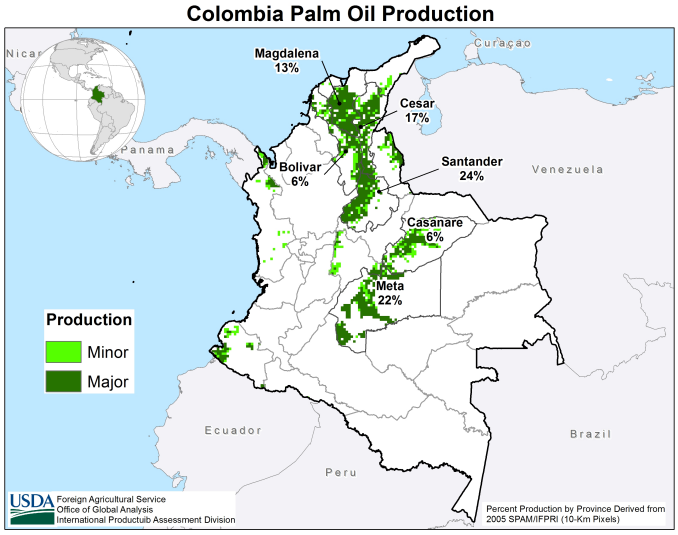

Figure A.2 | **Distribution of palm oil production.** Palm oil production for Colombia in green (USDA).

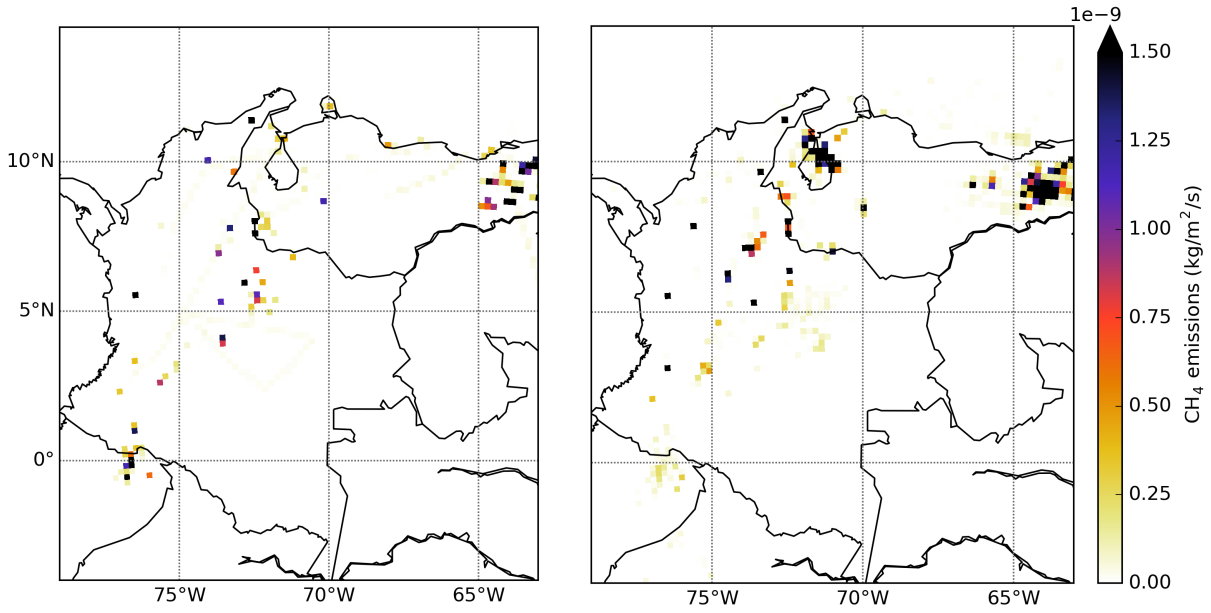

(a) EDGAR v4.3.2 **(b)** Scarpelli et al. (2018)

Figure A.3 | Comparison between fuel exploitation emissions of methane from EDGAR and Scarpelli. Methane emissions by fuel exploitation in $kg/m^2/s$ by EDGAR v4.3.2 (a) and Scarpelli et al. (2018) (b).

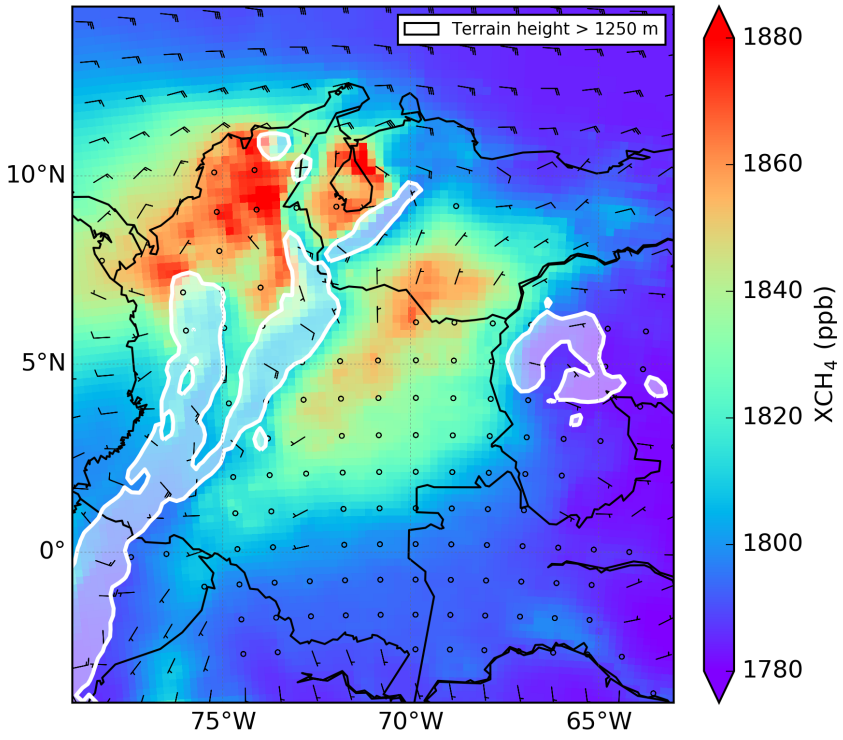

Figure A.4 | Simulated XCH_4 for August with the estimated emissions needed to match TROPOMI, including terrain height and wind. Simulated XCH_4 with WRF using the emissions that are estimated to match the observations by TROPOMI. Also the terrain height larger than 1250 meter and average wind is included.

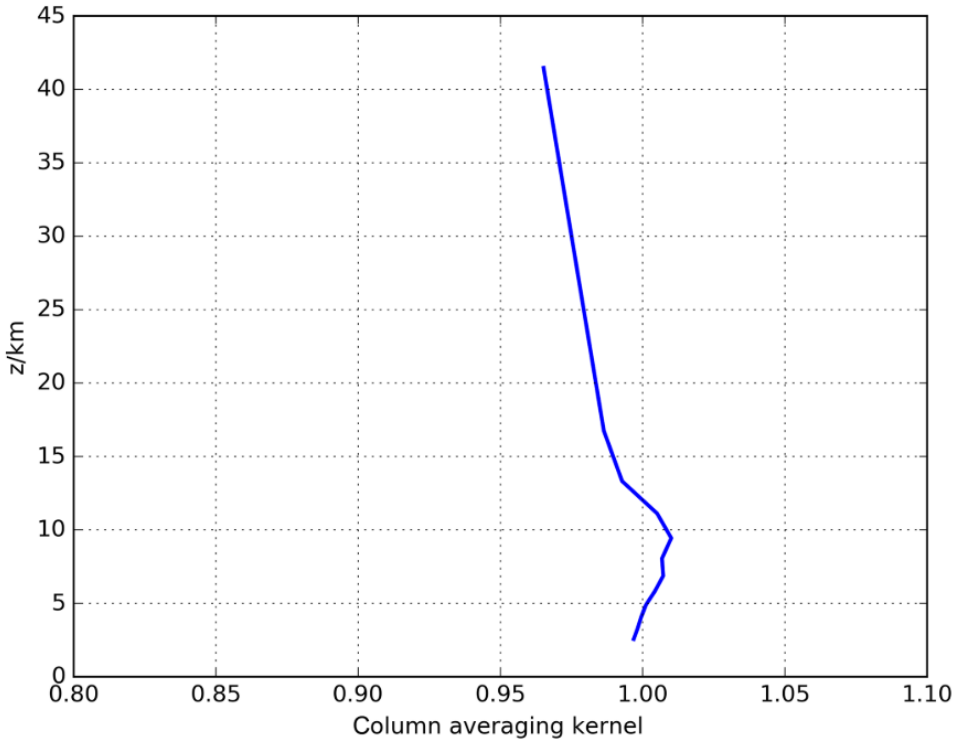

Figure A.5 | Column averaging kernel for a typical methane retrieval. Typical column averaging kernel for a methane retrieval by TROPOMI (Hu et al., 2016).